ELSEVIER

Separation and Purification Technology 21 (2000) 111–136

Separation and Purification Technology

www.elsevier.com/locate/seppur

Separation of hydrocarbon mixtures using zeolite membranes: a modelling approach combining molecular simulations with the Maxwell–Stefan theory

R. Krishna *, D. Paschek

Department of Chemical Engineering, University of Amsterdam, Nieuwe Achtergracht 166, 1018 WV Amsterdam, The Netherlands

Received 12 March 2000; received in revised form 8 April 2000; accepted 29 May 2000

Abstract

Zeolitic materials are often used for the separation of hydrocarbon mixtures. In this paper we suggest a procedure for modelling the separation performance using a combination of two techniques:

1. Configurational-bias Monte Carlo (CBMC) simulations for estimating the required pure component and mixture isotherms, and
2. Maxwell–Stefan formulation of mixture diffusion in zeolites.

The applicability of the suggested approach is demonstrated by comparing the theoretical predictions with experimental data published on zeolite membrane permeation. The theory provides clues to the development of new separation techniques and also for optimisation of the operating conditions.

Keywords: Configurational-bias Monte Carlo simulations; Maxwell–Stefan theory; Dual-site Langmuir isotherm; Real adsorbed solution theory; Zeolite membranes

Nomenclature

A	surface area of adsorbent, $m^2\ kg^{-1}$
b_i	parameter in the Langmuir adsorption isotherm, Pa^{-1}
$[B]$	square matrix of inverse Maxwell–Stefan coefficients, $m^{-2}\ s$
D_1	Fick's diffusivity of component 1 in zeolite, $m^2\ s^{-1}$
D_{12}	Fick's diffusivity of 1–2 binary in fluid mixture, $m^2\ s^{-1}$
$[D]$	matrix of Fick's diffusivities, m^2/s
$Đ_i$	Maxwell–Stefan's diffusivity of species i in zeolite, $m^2\ s^{-1}$

* Corresponding author. Tel.: +31-20-5257007; fax: +31-20-5255604.
E-mail address: krishna@its.chem.uva.nl (R. Krishna).

1383-5866/00/$ - see front matter
PII: S1383-5866(00)00196-9

$Đ_{12}$	Maxwell–Stefan's diffusivity of 1–2 binary in fluid mixture, $m^2\ s^{-1}$
$Đ_{ij}$	Maxwell–Stefan's diffusivity describing interchange between i and j, $m^2\ s^{-1}$
$D_{i,\mathrm{eff}}$	Effective Fick's diffusivity for component i diffusing in a zeolite, $m^2\ s^{-1}$
f_i	fugacity of species i; $f_i = p_i$ for ideal gases, Pa
$\mathbf{J}_i$	molar or molecular diffusion flux of species i relative to zeolite matrix, mol $m^{-2}\ s^{-1}$ or molecules $m^{-2}\ s^{-1}$
n	number of diffusing species, dimensionless
$\mathbf{N}_i$	molar or molecular flux of species i, mol $m^{-2}\ s^{-1}$ or molecules $m^{-2}\ s^{-1}$
$\mathbf{N}_t$	mixture molar or molecular flux, mol $m^{-2}\ s^{-1}$ or molecules $m^{-2}\ s^{-1}$
P	system pressure, Pa
P_i^0	vapour pressure analogue in Eq. (4), Pa
p_i	partial pressure of species i, Pa
q_i	adsorbed species molar concentration, mol kg^{-1}
$q_{i,\mathrm{sat}}$	total saturation concentration, mol kg^{-1}
R	gas constant, 8.314 J $mol^{-1}\ K^{-1}$
t	time, s
T	absolute temperature, K
$\mathbf{u}_i$	velocity of the diffusing species i, m s^{-1}
x_i	mole fraction of species i, dimensionless
z	number of nearest neighbour sites, dimensionless
z	distance coordinate along membrane, m

Greek letters

δ	thickness of membrane, m
γ_i	activity coefficient of species i, dimensionless
Γ	thermodynamic correction factor, dimensionless
$[\Gamma]$	matrix of thermodynamic factors, dimensionless
θ_i	fractional surface occupancy of component i
Θ_i	molecular loading, molecules per unit cell or per cage
$\Theta_{i,\mathrm{sat}}$	saturation loading, molecules per unit cell or per cage
$\Theta_{i,\mathrm{sat,A}}$	maximum loading of site A, molecules per unit cell
$\Theta_{i,\mathrm{sat,B}}$	maximum loading of site B, molecules per unit cell
λ	lateral displacement, m
Λ_{ij}	Wilson parameters, dimensionless
μ_i	molar chemical potential, J mol^{-1}
π	spreading pressure, Pa m
ν	jump frequency, s^{-1}
ρ	density of membrane, number of unit cells per m^3 or kg m^{-3}

Subscripts

A	refers to site A
B	refers to site B
1	component 1 in binary mixture
2	component 2 in binary mixture
max	refers to maximum loading
sat	refers to saturation conditions
i, j	components in mixture

eff	effective parameter
p	derivative at constant pressure
T,p	derivative at constant temperature and pressure
$n+1$	pseudo species

Superscripts

0	pure component parameter

Vector and matrix notation

( )	component vector
[ ]	square matrix

Operators

∇	gradient or nabla

1. Introduction

The separation of hydrocarbon mixtures is a problem of considerable practical importance. Materials such as silicalite, mordenite, NaX and NaY are often used for this purpose and separation is achieved by relying on the principle of selective sorption and diffusion within the zeolite structure [1]. There are fundamentally two ways in which the separation process can be realised, (a) using a packed bed adsorber [2] or (b) allowing the mixture to permeate across a supported zeolite membrane [3–5]. The packed bed adsorber operates essentially in an unsteady-state fashion whereas zeolite membrane permeation is essentially carried out in a steady-state manner. Sorption and diffusion are closely inter linked and for screening and design purposes we require information on the fluid mixture–zeolite equilibria (the mixture isotherm) and a method for calculating the diffusion fluxes of the individual species. In this paper we discuss a strategy for generating the required information by using (1) configurational-bias Monte Carlo (CBMC) simulations to develop the required mixture isotherms and (2) the Maxwell–Stefan theory for describing mixture diffusion across a zeolite membrane.

The major objective of this paper is to demonstrate the validity of this approach by comparing model predictions with published experimental data on zeolite membrane permeation. Furthermore, we shall show how this approach leads to development of novel separations.

2. CBMC simulations of pure component and mixture isotherms

While there is a considerable amount of published experimental data on pure component isotherms for various hydrocarbons [6,7], there is very little data on mixture isotherms. This lack of mixture isotherm data is most probably due to the difficulty of experimentation. Earlier publications [8–16] have shown the power of CBMC simulations for calculating pure component and mixture isotherms for normal and branched alkanes in silicalite and ferrierite. For linear and branched alkanes in silicalite, Vlugt et al. [15] have provided a detailed comparison of pure component isotherms estimated from CBMC techniques with published experimental data to demonstrate the accuracy of CBMC simulations. In this work we have carried out further pure component and mixture isotherm simulations in order to examine whether the mixture isotherms can be predicted on the basis of pure component isotherms. All the CBMC simulations reported here have been carried out for silicalite-1.

Our simulations have been performed in the grand canonical ensemble wherein the zeolite is in

contact with a reservoir that fixes the chemical potential of each component and also the temperature. In a CBMC simulation, it is essential to successfully exchange particles with the reservoir. With this technique we grow a flexible alkane molecule atom by atom in such a way that the 'empty spaces' in the zeolite are found. The bias of this growing scheme is removed exactly by a modification of the acceptance rules [13,15]. The acceptance ratio of the particle exchange move is increased by 10–100 orders of magnitude and thus makes these simulations possible. To increase the efficiency for the mixture simulations, we also performed trial moves which change the identity of a particle. In the simulations presented in this work the linear and branched alkanes are described with a united-atom model, i.e. CH_3, CH_2 and CH groups are considered to be single interaction centres. The zeolite is assumed to be rigid and the interactions of the alkane with the zeolite are dominated by the oxygen atoms of the zeolite. The alkane–zeolite and alkane–alkane interactions are described by a Lennard–Jones potential. The intra-inolecular interactions include bond-bending and torsion potentials and a fixed C–C bond length. The force-field parameters are reported in Vlugt et al. [15].

Our simulation box consists of 16 ($2 \times 2 \times 4$) unit cells of silicalite. The simulations are performed in cycles; in each cycle an attempt is made to perform one of the following moves, (1) displacement of a chain; a chain is selected at random and given a random displacement; (2) rotation of a chain; a chain is selected at random and given a random rotation around the centre of mass; (3) partial regrowing of a chain; a chain is selected at random and part of the molecule is regrown using the CBMC scheme; (4) exchange with reservoir using the CBMC scheme; it is decided at random whether to add or to remove a molecule from the zeolite; and (5) change of identity (only in the case of mixtures); one of the components is selected at random and an attempt is made to change its identity. The acceptance rules for this type of move are given elsewhere [13,15]. A total simulation consisted of at least 300 000 Monte Carlo cycles.

In order to illustrate various features of hydrocarbon mixture isotherm characteristics, we performed CBMC simulations for the following systems:

1. methane–ethane;
2. methane–propane;
3. ethane–propane;
4. n-butane–iso-butane;
5. n-hexane–3-methyl pentane (3MP);
6. n-hexane–2,2 dimethyl butane (22DMB);
7. iso-butane–propane;
8. n-pentane–2-methyl pentane (2MP).

For mixtures a, b and c the components of the mixture differ in size, i.e. the number of C atoms. Mixtures d, e and f consist of hydrocarbon isomers with linear and branched alkanes having the same number of C atoms; these mixtures have different molecular configurations. Mixtures g and h consist of linear and branched alkanes with differing number of C atoms; here both size and configuration effects play a role. In all the above cases we performed CBMC simulations of the constituent pure components and of the mixtures.

2.1. Modelling the pure component isotherms

For the pure component linear and branched alkanes studied here, the dual-site Langmuir (DSL) model was found to be applicable in all the cases. The DSL model for the loading, expressed in molecules per unit cell, is

$$\Theta_i^0(P) = \frac{\Theta_{i,\mathrm{sat,A}} b_{i,\mathrm{A}} P}{1 + b_{i,\mathrm{A}} P} + \frac{\Theta_{i,\mathrm{sat,B}} b_{i,\mathrm{B}} P}{1 + b_{i,\mathrm{B}} P} \tag{1}$$

gives a good description of the pure component isotherms. The superscript 0 on $\Theta_i^0(P)$ is used to emphasise that the relation is for *pure* component loadings. For silicalite-1 a molecular loading of four molecules per unit cell corresponds to 0.6935 mol kg^{-1} and therefore the molar loading, $q_i^0(P)$, is given by the following expression

$$q_i^0(P) = \Theta_i^0(P) \times 0.1734 \tag{2}$$

In Eq. (1) the subscripts A and B refer to two sorption sites within the silicalite structure, with different sorption capacities and sorption strengths. The fitted parameters for the pure component isotherms are listed in Table 1. With in-

creasing number of carbon atoms the saturation capacity, $\Theta_{i,sat} = \Theta_{i,sat,A} + \Theta_{i,sat,B}$, decreases; see Fig. 1. The fitted DSL isotherms for linear and branched (2-methyl) alkanes for C numbers ranging from 1–9 are shown in Fig. 2. All the branched alkanes show inflection at a loading of four molecules per unit cell because these molecules prefer to locate at the channel intersections (see Fig. 3) rather than within the channel interiors. An extra 'push', i.e. pressure is required

Table 1
Pure component parameters for dual-site Langmuir model

Component i	Temperature/K	Dual-site Langmuir parameters, see Eq. (1)			
		Site A		Site B	
		$b_{i,A}$/Pa^{-1}	$\Theta_{i,sat,A}$/molecules per unit cell	$b_{i,B}$/Pa^{-1}	$\Theta_{i,sat,B}$/molecules per unit cell
Methane	300	4.86×10^{-6}	11.0	2.38×10^{-7}	8.0
	303	4.6×10^{-6}	11.0	2.0×10^{-7}	8.0
Ethane	300	9.73×10^{-5}	12.0	4.38×10^{-7}	3.0
	303	8.28×10^{-5}	12.0	3.73×10^{-7}	3.0
Propane	300	9.64×10^{-4}	11.0	5.06×10^{-6}	1.0
	303	7.95×10^{-4}	11.0	1.59×10^{-6}	1.0
n-Butane	300	1.6×10^{-2}	9.0	1.1×10^{-5}	1.0
iso-Butane	300	2.84×10^{-2}	4.0	4.3×10^{-6}	6.0
n-Pentane	300	0.218	8.0	1.95×10^{-5}	0.5
n-Hexane	362	6.32×10^{-2}	4.0	1.7×10^{-3}	4.0
	373	3.29×10^{-2}	4.0	8.1×10^{-4}	4.0
	398	8.1×10^{-3}	4.0	1.6×10^{-4}	4.0
2-Methyl pentane	300	5.286	4.0	1.22×10^{-5}	2.2
3-Methyl pentane	362	4.75×10^{-2}	4.0	2.27×10^{-5}	2.3
2,2 Dimethyl butane	373	5.67×10^{-3}	4.0		0
2,2 Dimethyl butane	398	1.6×10^{-3}	4.0		0

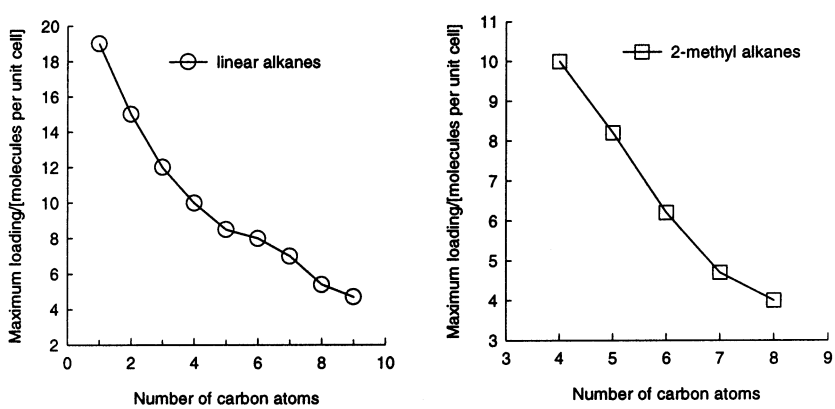

Fig. 1. Saturation loadings (molecules per unit cell) of alkanes in silicalite-1 obtained from CBMC simulations.

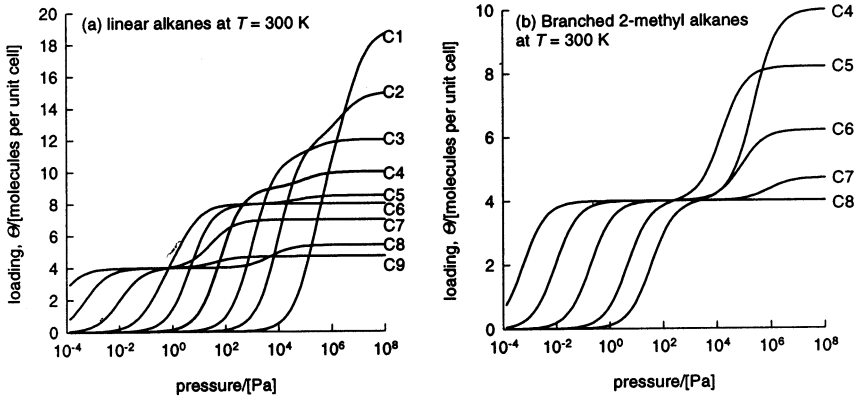

Fig. 2. Pure component isotherms for (a) linear and (b) 2-methyl-alkanes in silicalite-1 at 300 K calculated using CBMC.

to make these occupy the interiors. This gives rise to the inflection. For linear alkanes with six or more C atoms, we observe an inflection at a loading of four molecules per unit cell.

Both differences in the saturation capacities and molecular configurations are important determinants of the sorption selectivity in the mixture, defined by

$$\text{Sorption selecivity} = \frac{\Theta_1/\Theta_2}{p_1/p_2} \tag{3}$$

In Eq. (3) Θ_i refers to the loadings of the components in the mixture within the zeolite.

2.2. Modelling the mixture isotherms using IAS and RAS theories

The mixture loadings can also be estimated from the pure component isotherms using the ideal adsorbed solution (1AS) theory of Myers and Prausnitz [17]. Briefly, the basic equation of IAS is the analogue of Raoult's law for vapour–liquid equilibrium, i.e.

$$Py_i = P_i^0(\pi)x_i \tag{4}$$

where, x_i is the mole fraction in the adsorbed phase

$$x_i = \frac{\Theta_i}{\Theta_1 + \Theta_2} \tag{5}$$

and $P_i^0(\pi)$ is the pressure for sorption of every pure component i, which yields the same spreading pressure, π, as that for the mixture. The spreading pressure is defined by the Gibbs adsorption isotherm

$$\frac{\pi A}{RT} = \int_{P=0}^{P=P_i^0} \frac{q_i^0(P)}{P}\,\mathrm{d}P \tag{6}$$

where A is the surface area of the adsorbent and $\Theta_i^0(P)$ is the pure component isotherm given by Eq. (1). The total amount adsorbed is obtained from

$$\Theta_1 + \Theta_2 = \frac{1}{x_1/\Theta_1^0(P_1^0) + x_2/\Theta_2^0(P_2^0)} \tag{7}$$

The set of Eqs. (1), (4)–(7) need to be solved numerically to obtain the mixture loadings of components 1 and 2.

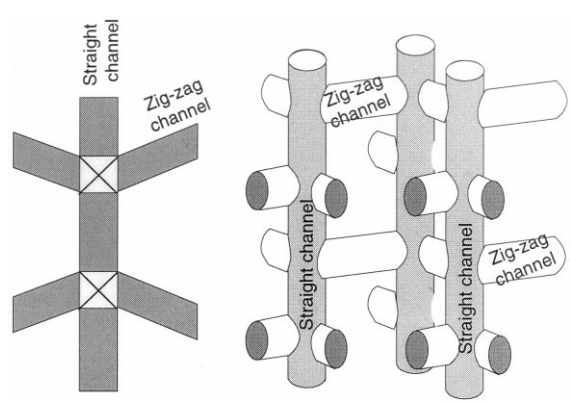

Fig. 3. Sorption sites within silicalite.

Table 2
Wilson non-ideality parameters for mixture isotherms

Mixture	Temperature/K	Wilson parameters	
		Λ_{12}	Λ_{12}
(a) Methane –ethane	303	1	1
(b) Methane –propane	303	1	1
(c) Ethane –propane	300	1	1
(d) n-Butane –iso-butane	300	6.95	1.005
(e) n-Hexane –3-methyl pentane	362	1.01	0.215
(f) n-Hexane–2,2 dimethyl butane	373	2.6	0.01
	398	2.6	0.01
(g) iso-Butane –propane	300	9.6	4.27
(h) n-Pentane –2-methyl pentane	300	1.416	15.83

On the basis of the CBMC mixture simulations we can establish that for mixtures (d)–(h) the IAS theory is not adequate to describe the mixture behaviour and that non-ideality effects need to be taken into account. The mixture non-ideality effects can be quantified by the introduction of activity coefficients into Eq. (4). The resulting real adsorbed solution (RAS) theory is described by

$$Py_i = P_1^0(\pi)x_i\gamma_i \tag{8}$$

Following the work of Calleja et al. [18] we have used the Wilson model for the activity coefficients:

$$\ln(\gamma_1) = 1 - \ln(x_1 + x_2\Lambda_{12}) - \frac{x_1}{x_1 + x_2\Lambda_{12}} - \frac{x_2\Lambda_{21}}{x_2 + x_1\Lambda_{21}}$$

$$\ln(\gamma_2) = 1 - \ln(x_2 + x_1\Lambda_{21}) - \frac{x_2}{x_2 + x_1\Lambda_{21}} - \frac{x_1\Lambda_{12}}{x_1 + x_2\Lambda_{12}} \tag{9}$$

The values of the fitted Wilson parameters are given in Table 2. We now discuss the various features of the mixture isotherms studied.

2.3. CBMC mixture simulations

CBMC simulation results for pure component and mixture loadings for methane–ethane at 303 K are shown in Fig. 4a and b. The mixture loadings obtained from CBMC simulations show excellent agreement with the predictions of the IAS theory; see Fig. 4b. At high loadings within the zeolite, the smaller sized methane (with a higher saturation capacity) is preferred because the vacant spaces in the zeolite can be more efficiently filled up with methane molecules than with ethane. This is a *size entropy* effect [8,19]. The sorption selectivity towards ethane decreases with increasing partial pressure of ethane due to size entropy effects; see Fig. 4c.

The pure component and mixture loadings for methane–propane determined by CBMC simulations at 303 K are shown in Fig. 5a and b. The size entropy effects for methane–propane mixtures are more significant than that for methane–ethane. This is illustrated in Fig. 5c which shows that the sorption selectivity towards propane decreases significantly with increasing partial pressure of propane in the bulk gas phase. The predictions of the IAS theory are again in excellent agreement with the CBMC calculations for the mixture loadings; see Fig. 5b.

The pure component and mixture loadings for ethane–propane determined by CBMC simulations at 300 K are shown in Fig. 6a and b). The size entropy effects for ethane–propane mixtures are less significant than that for methane–propane and there is a slight decrease in propane sorption selectivity with increasing partial pressure of propane in the bulk gas phase; see Fig. 6c. The predictions of the IAS theory are once again in excellent agreement with the CBMC calculations for the mixture loadings; see Fig. 6b.

The pure component and mixture loadings for n-butane–iso-butane determined by CBMC simulations at 300 K are shown in Fig. 7. The pure

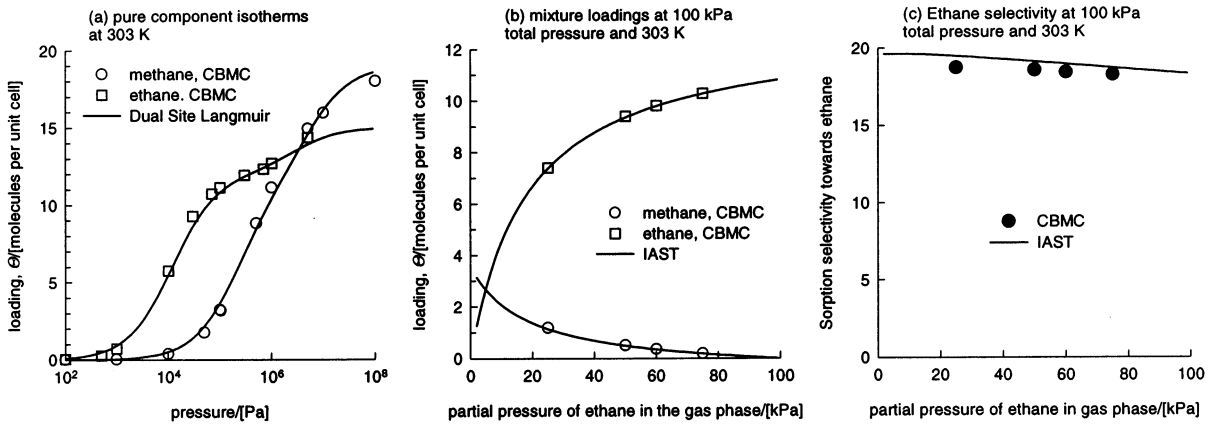

Fig. 4. Pure component and mixture loadings for methane (1)–ethane (2) at 303 K in silicalite.

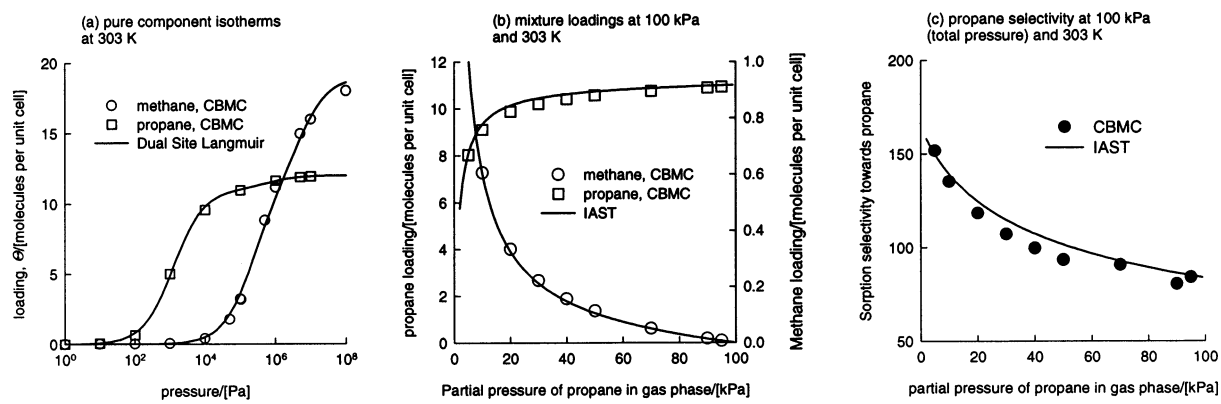

Fig. 5. Pure component and mixture loadings for methane (1)–propane (2) at 303 K in silicalite.

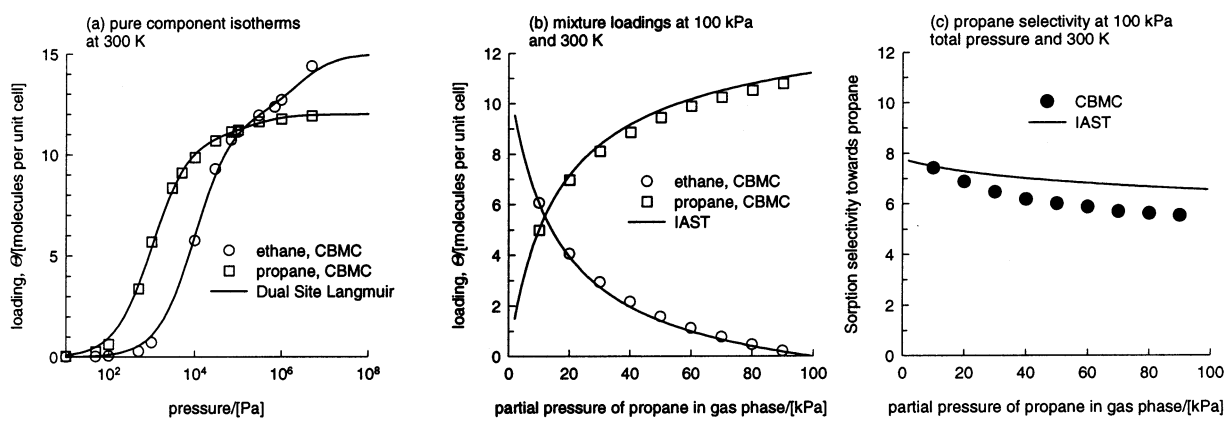

Fig. 6. Pure component and mixture loadings for ethane (1)–propane (2) at 300 K in silicalite.

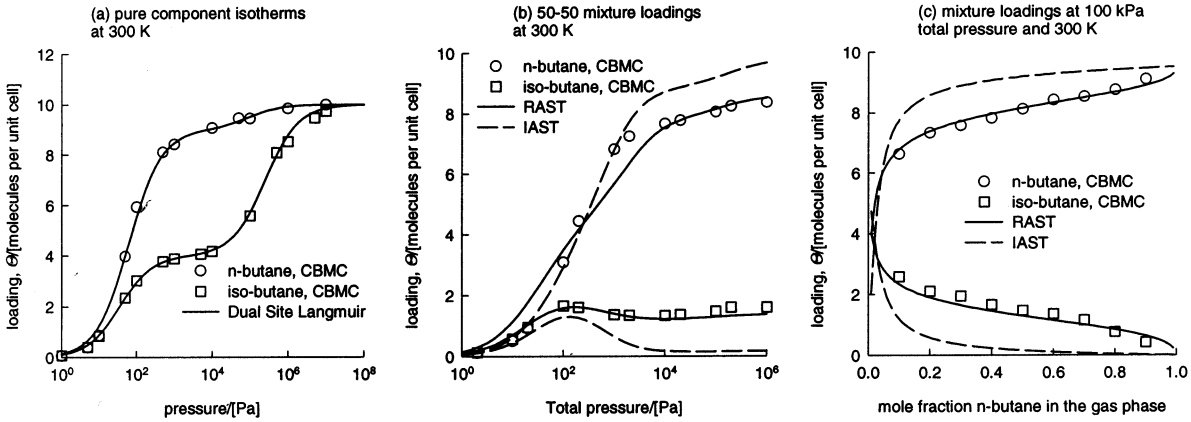

Fig. 7. Pure component and mixture loadings for n-butane (1)–iso-butane (2) at 300 K in silicalite.

component isotherm for iso-butane shows a pronounced inflection at a loading of four molecules per unit cell; see Fig. 7a. This inflection behaviour has been explained in earlier work [14] and is due to the fact that the iso-butane molecules prefer to locate at the channel intersections and require an extra 'push' to make these occupy the channel interiors. The normal butane molecules, on the other hand, have no particular preference for either the channel intersections or interiors.

CBMC simulations of the loadings of normal and iso-butane are shown in Fig. 7b for a 50–50 mixture and in Fig. 7c at varying bulk fluid compositions. Contrary to the three mixtures studied earlier, the mixture loadings do not agree with the predictions of the IAS theory. Apparently, non-ideality effects begin to play a role. The reason for the non-ideality can be understood by examining a snapshot of the location of the molecules at a total pressure of 1000 kPa and 300 K; see Fig. 8. We see that the iso-butane molecules are located only at the intersections. However, due to the specific size of the molecules, the n-butane molecules are slightly displaced along the channel interiors. A consequence of this is that the n-butane molecules 'stick out' into the adjoining intersection site. Every other intersection site is not available for accommodating either molecule. The RAST and IAST predictions of the mixture loadings are compared with CBMC simulations in Fig. 7b and c. We note that the mixture non-ideality effects are quite significant. In Fig. 7b we also note that the branched alkane shows a maximum in the loading; this maximum occurs precisely at a total mixture loading of four molecules per unit cell.

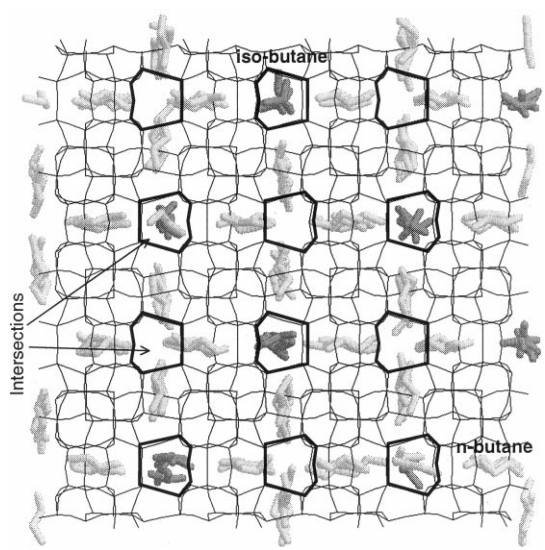

Fig. 8. Snapshot showing the location of n-butane (1)–iso-butane (2) at 300 K and 1000 kPa in silicalite. The view is in the z direction.

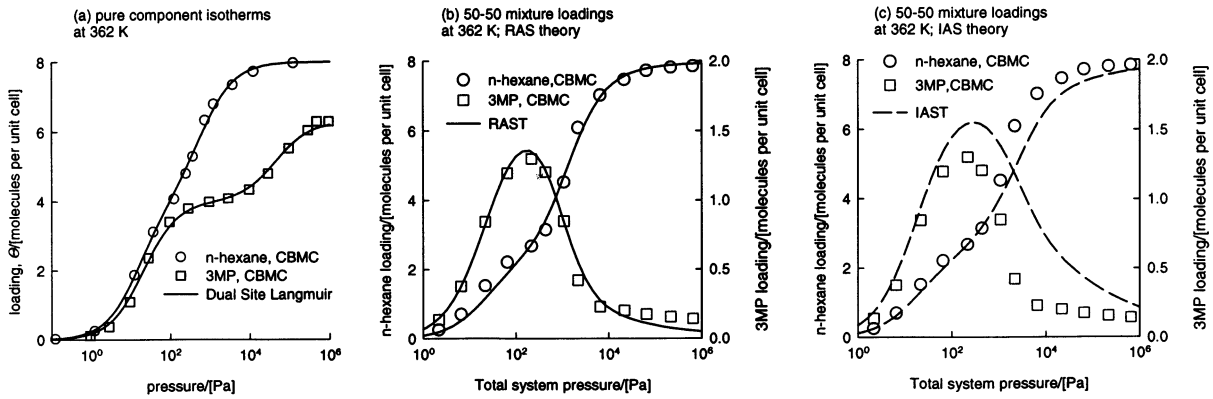

Fig. 9. Pure component and mixture loadings for n-hexane (1)–3MP(2) at 362 K in silicalite.

The pure component and mixture isotherms for n-hexane and 3-methyl pentane calculated from CBMC simulations are compared with both IAST and RAST predictions in Fig. 9. The branched alkane 3MP exhibits a curious maximum with respect to molecular loading within the silicalite structure. As the partial pressures increase to 100 Pa, the sorbate loading of both linear and branched alkanes increase till a maximum is reached in the loading of 3MR. This occurs at a total loading of four molecules per unit cell. Up to this point there is really no competition between n-C_6 and 3MP and both are almost equally easily adsorbed.

Examination of a snapshot of the molecular sittings at 100 Pa shows that all the 3MP molecules are located at the intersections between the straight channels and the zigzag channels whereas n-C_6 are located everywhere; see Fig. 10. The n-C_6 molecules fit nicely into both straight and zigzag channels [12], these molecules have a higher 'packing efficiency' than 3MR. As the pressure is increased beyond 100 Pa, it is more efficient to obtain higher loading by 'replacing' the 3MP with n-C_6; this *configurational entropy* effect is the reason behind the curious maximum in the 3MP isotherm.

We note from Fig. 9b and c that mixture non-ideality effects are present and that the CBMC simulations show a stronger exclusion of 3MP at high pressures than anticipated by the IAS theory. For prediction of separation selectivities non-ideality effects must clearly be taken into account; we return to this point later during our discussions on membrane permeation.

For the mixture n-hexane–22DMB, a similar result is obtained [11]. CBMC simulations at 373 and 398 K are shown in Figs. 11 and 12, respectively. Again we note the maximum in the 22DMB loading when the mixture loading corresponds to four molecules per unit cell. The Wilson non-ideality parameters for the 373 and 398 K simulations are the same showing, at least for the temperature ranges studied, the non-ideality ef-

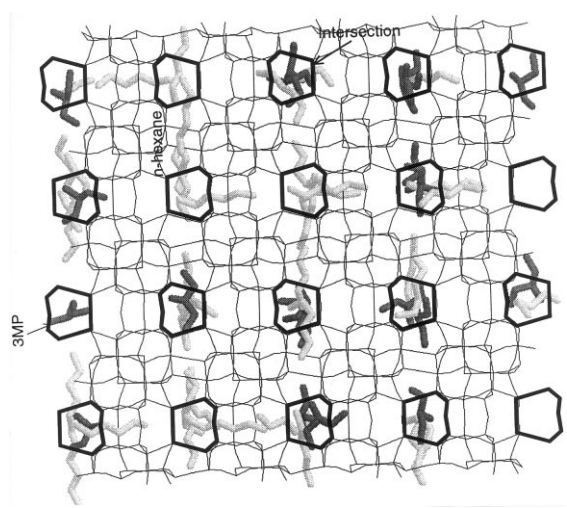

Fig. 10. Snapshot showing the location of a 50–50 mixture of n-hexane (1)–3MP (2) at 362 K and 100 Pa. Preferential siting of 3 MP alkanes at the intersections between the straight and zigzag channels is evident. The linear alkane can be located at any position within the silicalite structure.

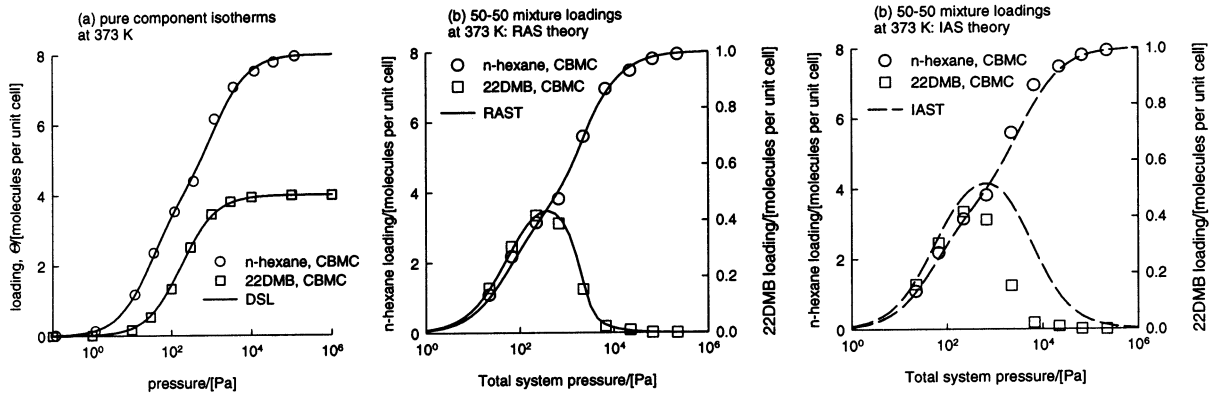

Fig. 11. Pure component and mixture loadings for n-hexane (1)–22DMB (2) at 373 K in silicalite.

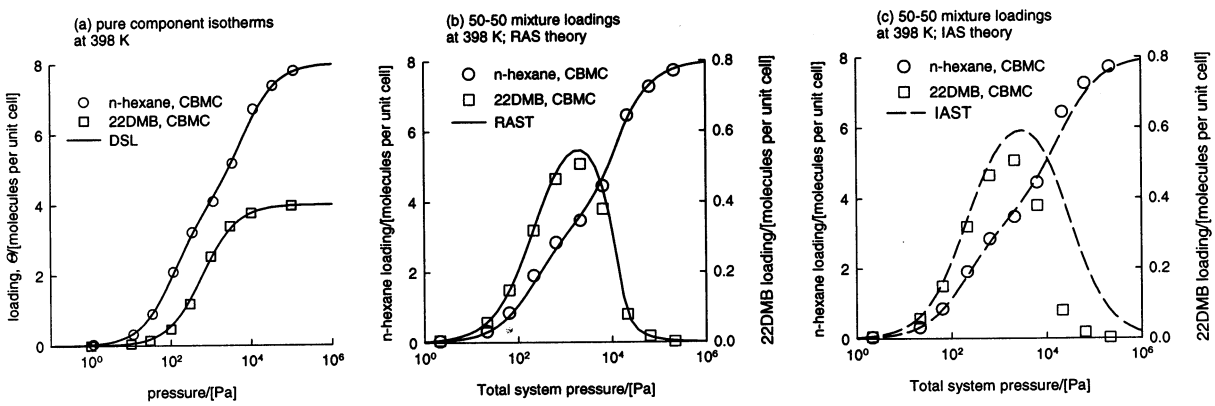

Fig. 12. Pure component and mixture loadings for n-hexane (1)–22DMB (2) at 398 K in silicalite.

fects are not strongly temperature dependent; this is a useful conclusion. Non-ideality effects are important to describe the mixture isotherms; we will see later in this paper that such non-ideality effects have a significant effect on the permeation fluxes across a silicalite membrane.

CBMC simulations of iso-butane–propane and n-pentane–2MP are shown in Figs. 13 and 14, respectively. These mixtures differ both in the number of C atoms and in the molecular configuration. The mixture non-ideality effects can be expected to be stronger than for the other systems considered above. This is indeed found to be the case; compare the Wilson parameters in Table 2.

Having described the fluid–zeolite equilibria, we turn to the description of diffusion of hydrocarbon mixtures within the zeolite structure.

3. The Maxwell–Stefan theory for diffusion

3.1. Points of departure from fluid phase diffusion

When describing diffusion within a zeolite, there are several points where we depart from the conventional treatment of bulk fluid phase diffusion [20,21].

1. First, when we consider movement of species within a zeolite structure, it is important to realise that we are talking of movement of *sorbed* species. Diffusion and sorption processes within zeolites are closely inter-twined.
2. Secondly, when describing the diffusion of a mixture of n species within a zeolite, the 'zeolite matrix' is treated as an additional (pseudo), $(n+1)$th component, in the mixture.

So, when we speak, say, about diffusion of benzene (component 1) within silicalite we are in fact considering diffusion in a binary mixture made up of benzene (component 1) and silicalite (pseudo-component 2).

3. The third point concerns the concentration measures. Commonly used concentration measures for sorption are (1) mol of sorbate (diffusant) per kg of zeolite, q_i, and (2) molecules of sorbate per unit cell of zeolite, Θ_i. Corresponding to these two concentration measures we could define the molar flux $\mathbf{N}_i$ in two different ways. The first alternative is in terms of moles of sorbate diffusing per square meter per second:

$$\mathbf{N}_i \equiv \rho q_i \mathbf{u}_i; \quad i = 1,\ 2,\ \ldots,\ n-1 \tag{10}$$

where ρ is the zeolite matrix density expressed in kg m^{-3}. The second alternative is to define $\mathbf{N}_i$ in terms of molecules transported per square meter per second

$$\mathbf{N}_i \equiv \rho \Theta_i \mathbf{u}_i; \quad i = 1,\ 2,\ \ldots,\ n-1 \tag{11}$$

in which case ρ is the zeolite matrix density expressed as unit cells per m^3. Without loss of generality we proceed further with the choice of Θ_i, as the concentration measure; relations in terms q_i can be written down in an analogous manner.

4. The fourth point of departure from bulk fluid phase diffusion concerns the choice of the

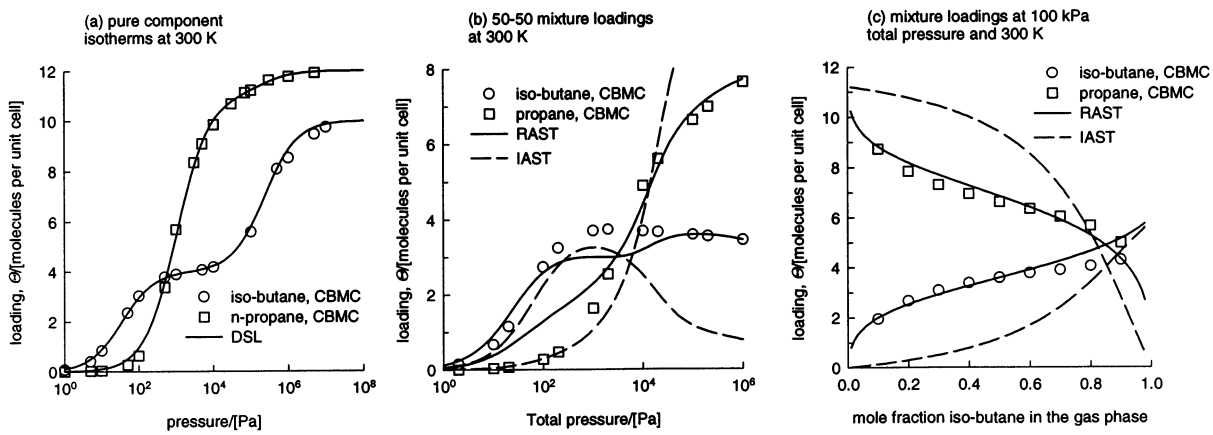

Fig. 13. Pure component and mixture loadings for iso-butane (1)–propane (2) at 300 K in silicalite.

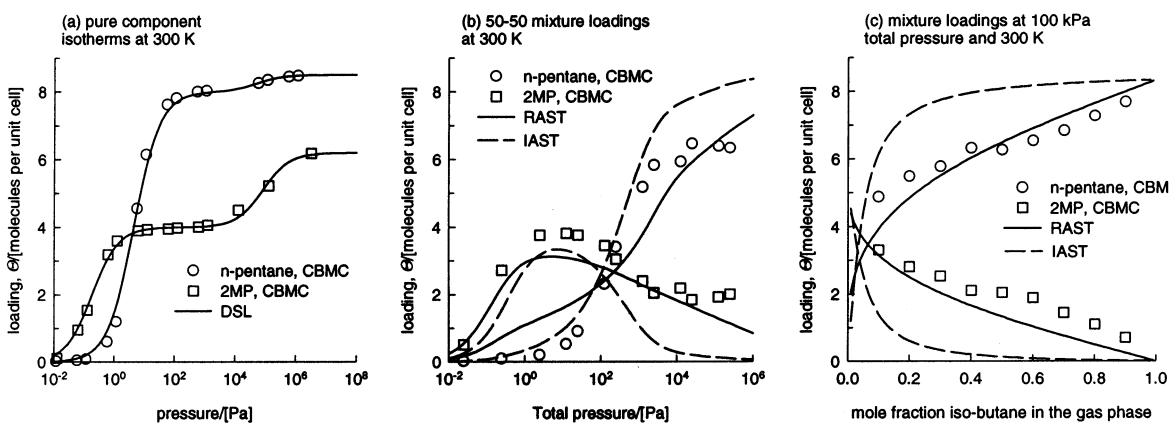

Fig. 14. Pure component and mixture loadings for n-pentane (1)–2MP (2) at 300 K in silicalite.

reference frame for defining the diffusion fluxes $\mathbf{J}_i$. In almost all standard treatments of diffusion in zeolites [22,23], the reference velocity frame is *tacitly* chosen as one which moves with respect to the zeolite matrix, taken to be the $(n+1)$th component. The diffusion fluxes are therefore defined as

$$\mathbf{J}_i \equiv \rho \Theta_i (\mathbf{u}_i - \mathbf{u}_{n+1}); \quad i = 1,\ 2,\ \ldots,\ n \tag{12}$$

In most of the applications of interest to chemical engineers the zeolite matrix can be considered to be stationary, i.e.

$$\mathbf{u}_{n+1} \equiv 0 \tag{13}$$

Eq. (14) implies that molar flux $\mathbf{N}_i$ equals the diffusion flux $\mathbf{J}_i$:

$$\mathbf{J}_i \equiv \mathbf{N}_i \equiv \rho \Theta_i \mathbf{u}_i \tag{14}$$

5. The fifth point concerns the choice of a composition measure analogous to the mole fraction for bulk fluid phases. The obvious choice is the fractional occupancy θ_i of the sorbate within the zeolite matrix, defined as

$$\theta_i \equiv \frac{\Theta_i}{\Theta_{i,\mathrm{sat}}} = \frac{q_i}{q_{i,\mathrm{sat}}}; \quad i = 1,\ 2,\ \ldots,\ n \tag{15}$$

where $\Theta_{i,\mathrm{sat}}$, and $q_{i,\mathrm{sat}}$, are the saturation loadings of species i in the zeolite.

3.2. Diffusion of a single component in a zeolite

Let us first consider the simple case of diffusion of a single component (1) within a zeolite (considered to be pseudo-species (2). Fick's law is usually written in the following form:

$$\mathbf{N}_1 = -\rho D_1 \nabla \Theta_1 \tag{16}$$

or in terms of the occupancy gradients

$$\mathbf{N}_1 = -\rho \Theta_{1,\mathrm{sat}} D_1 \nabla \theta_1 \tag{17}$$

Eq. (16) or Eq. (17), defines the Fick diffusivity D_1. The Fick diffusivity, D_1, is also called the *transport diffusivity* in the zeolite literature [22,23].The Maxwell–Stefan formulation [24–30] of single component diffusion is

$$\mathbf{N}_1 = -\rho \Theta_{1,\mathrm{sat}} Đ_1 \left(\frac{\theta_1}{RT} \nabla \mu_1 \right) \tag{18}$$

where μ_1 is the chemical potential of the sorbed species 1. Assuming equilibrium between the sorbed species and the bulk fluid phase we have the following relationship for the chemical potential μ_1

$$\mu_1 = \mu_1^0 + RT \ln(f_1) \tag{19}$$

where μ_1^0 is the chemical potential in the chosen standard state and f_1 is the fugacity. For not too high system pressures the component partial pressure, p_1, can be used in place of the component fugacity, f_1, i.e. $f_1 \approx p_1$. The chemical potential gradients may be expressed in terms of the gradients of the occupancy, $\nabla\theta_1$,

$$\frac{1}{RT} \nabla \mu_1 = \frac{1}{\theta_1} \Gamma \nabla \theta_1; \quad \Gamma \equiv \theta_1 \frac{\partial \ln p_1}{\partial \theta_1} \tag{20}$$

where Γ is the thermodynamic correction factor. The Fick and Maxwell–Stefan diffusivities are therefore inter-related:

$$D_1 = Đ_1 \Gamma; \quad Đ_1 = \frac{D_1}{\Gamma} \tag{21}$$

In the zeolite diffusion literature the Maxwell–Stefan diffusivity $Đ_1$ is also called the 'corrected' diffusivity and the thermodynamic correction factor Γ is called the Darken correction factor [22,23,31].

Consider the sorption data for benzene in silicalite-1 [32] at a temperature $T = 343$ K (Fig. 15a). The experimental data are reasonably well represented by the Langmuir isotherm

$$\Theta_1 = \frac{\Theta_{1,\mathrm{sat}} b_1 P}{1 + b_1 P}; \quad \theta_1 = \frac{b_1 P}{1 + b_1 P} \tag{22}$$

where the saturation capacity $\Theta_{1,\mathrm{sat}}$ is four molecules per unit cell of silicalite and the Langmuir constant $b_1 = 6 \times 10^{-4}$ Pa^{-1}. The thermodynamic correction factor can be determined from Eq. (20)

$$\Gamma = \frac{1}{1 - \Theta_1/\Theta_{1,\mathrm{sat}}} = \frac{1}{1 - \theta_1} \tag{23}$$

Fig. 15b shows the variation of the thermodynamic factor with molecular loading. Notice the sharp increase in Γ as Θ_1 approaches the satura-

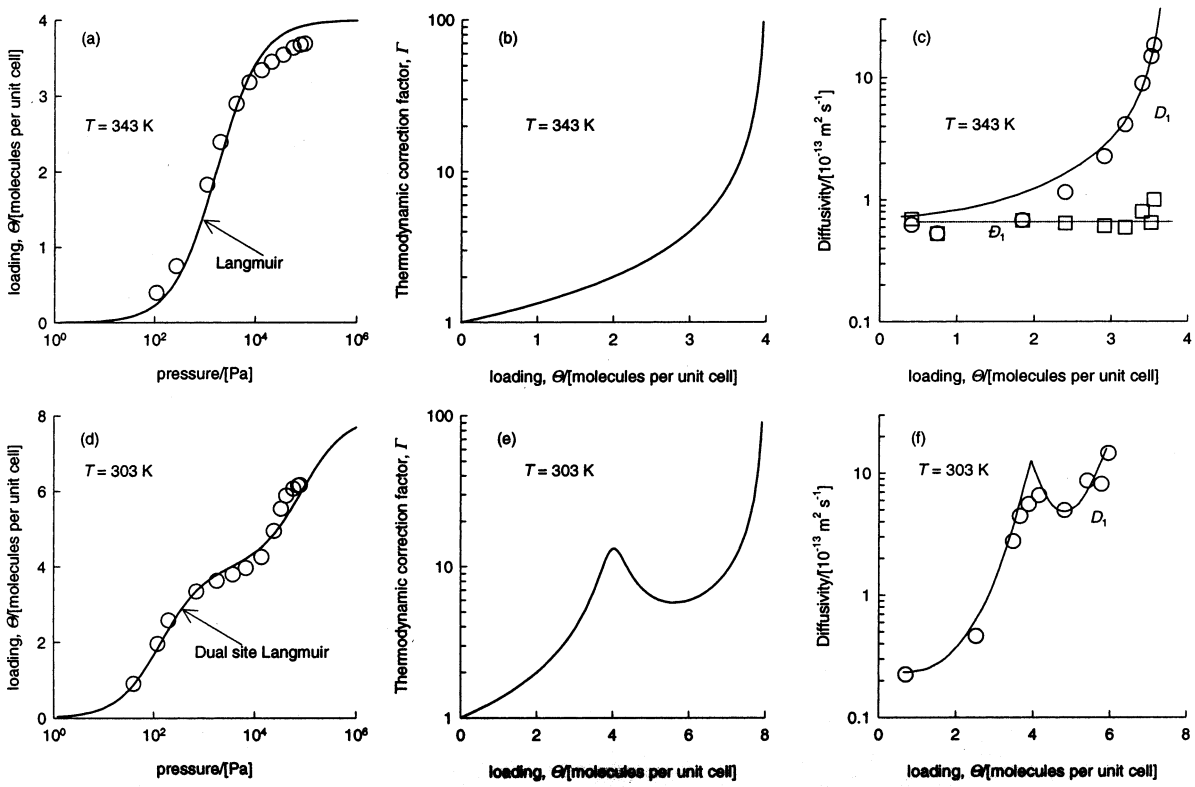

Fig. 15. (a) Pure component isotherms for sorption of benzene on silicalite-1 at a temperature of 343 K. Experimental data from Guo et al. [32]. The Langmuir model parameters are $\Theta_{1,sat} = 4$, $b_{1,A} = 6 \times 10^{-4}$ Pa^{-1}. (b) The thermodynamic correction factor calculated using the Langmuir model. (c) Fick and Maxwell–Stefan diffusivity data for benzene in silicalite-1 at 343 K. Data from Shah et al. [33]. (d) Pure component isotherms for sorption of benzene on silicalite-1 at a temperature of 303 K. Experimental data from Guo et al. [32]. The dual-site Langmuir model parameters are $\Theta_{sat,A} = 4$, $\Theta_{sat,B} = 4$, $b_{1,A} = 7 \times 10^{-3}$ Pa^{-1}, $b_{1,B} = 1.2 \times 10^{-5}$ Pa^{-1} (e) The thermodynamic correction factor calculated using the Langmuir model. (f) Fick's diffusivity data for benzene in silicalite-1 at 303 K. Data from Shah et al. [33].

tion capacity, $\Theta_{1,sat}$ ($=4$). The Fick diffusivity data for benzene in silicalite-1 measured by Shah et al. [33] is shown in Fig. 15c and is seen to parallel the behaviour of Γ. As seen in Fig. 15c, D_1 increases sharply as Θ_1 approaches the saturation capacity, $\Theta_{1,sat}$ ($=4$). The Maxwell–Stefan diffusivity $Đ_1$, displays a much smaller variation with sorbate loading; see the square symbols in Fig. 15c.

Fig. 15d shows the isotherm data for benzene in silicalite-1 at $T = 303$ K; the inflection at $\Theta =$ four molecules per unit cell is evident. The DSL model (Eq. (1)) provides a good description for systems showing isotherm inflection and the thermodynamic correction factor Γ can be determined by analytic differentiation of Eq. (1). This correction factor shows two extrema — a maximum at the inflection point $\Theta_{1,sat,A} = 4$ and a minimum at a loading $\Theta_{1,sat,A} < \Theta_1 < \Theta_{1,sat} (= \Theta_{1,sat,A} + \Theta_{1,sat,B})$. This behaviour is illustrated for adsorption of benzene on silicalite at temperatures of 303 K; see Fig. 15e. Since the Fick diffusivity is proportional to the thermodynamic factor, it can also be expected to exhibit two extrema. This is indeed verified by the experimental data of Shah et al. [33]; see Fig. 15f.

The thermodynamic correction factors for linear and branched alkanes at 300 K are shown in Fig. 16. Since the Fick diffusivity D_1 is expected to follow the trend in Γ we would expect to see striking differences between the occupancy dependency of the Fick diffusivities of say n-hexane and its isomer 2-methyl pentane as a function of the molecular loading. It would be most illuminating to obtain experimental confirmation of this prediction.

A three-site model for sorption of aromatics on ZSM-5 has been proposed by Rudzinski et al. [34] in order to account for two inflection points observed under certain temperature conditions. The consequences for diffusion can be expected to be interesting but there is no experimental evidence in the literature.

3.3. The Maxwell–Stefan diffusivity

Mechanistically, the Maxwell–Stefan diffusivity $Đ_1$, may be related to the displacement of the adsorbed molecular species, λ, and the jump frequency, ν, which in general can be expected to be dependent on the total coverage [35–39]

$$Đ_1 = \frac{1}{z}\lambda^2\nu \tag{24}$$

where z represents the number of nearest neighbour sites. The jump frequency ν can be expected to decrease with occupancy. If we assume that a molecule can migrate from one site to another only when the receiving site is vacant [31,38], the chance that this will occur will be a function of the fraction of unoccupied sites. A general form

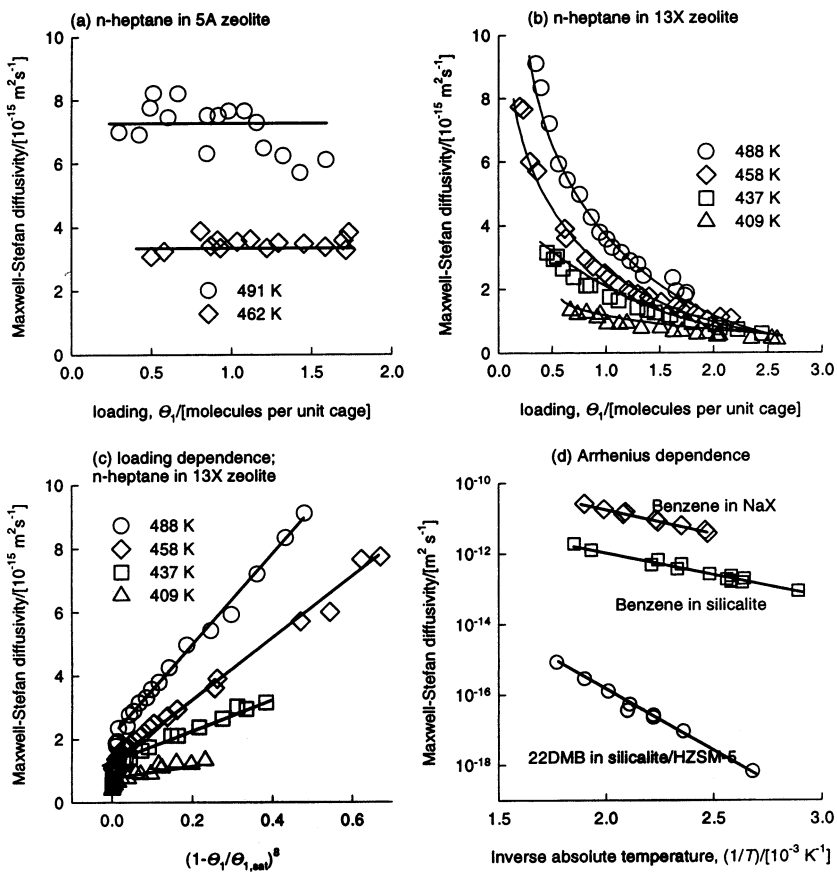

Fig. 16. (a) Thermodynamic factor for linear alkanes in silicalite-1 at 300 K calculated using the dual-site Langmuir (DSL). (b) Thermodynamic factor for 2-methyl alkanes in silicalite-1 at 300 K calculated using the dual-site Langmuir (DSL) model.

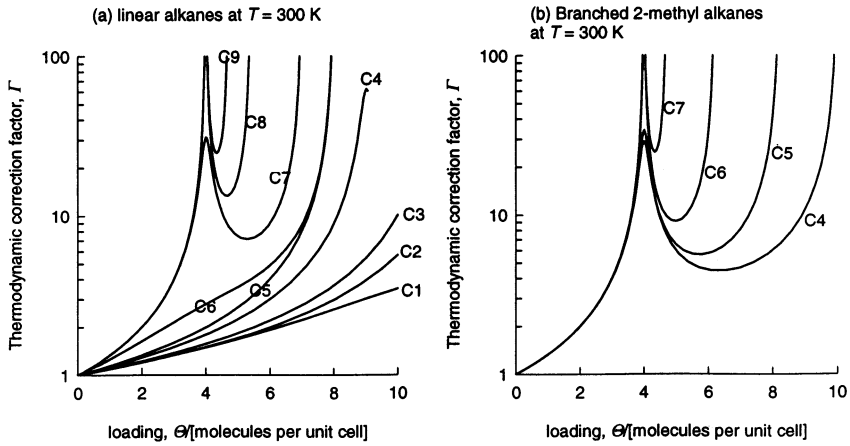

Fig. 17. (a) Maxwell–Stefan diffusivity data for n-heptane in 5A zeolite as a function of molecular loading. Data from Ruthven and Doetsch [40]. (b) Maxwell–Stefan diffusivity data for n-heptane in 13X zeolite as a function of molecular loading. Data from Ruthven and Doetsch [40]. (c) Re-plotting of the data in (b) for Maxwell–Stefan diffusivity for n-heptane in 13X zeolite in order to test the validity of the model proposed in Eq. (27). (d) Arrhenius plot for the Maxwell–Stefan diffusivity. Various data sources cited in the review by Ruthven and Post [41].

of the Maxwell–Stefan diffusion equation is therefore

$$Đ = Đ_1(0) f(1-\theta_1) \tag{25}$$

where, $Đ_1(0)$ represents the Maxwell–Stefan diffusivity in the limit of zero loading and $f(1-\theta_1)$ is some function of the fraction unoccupied sites.

The simplest model for the dependence of the Maxwell–Stefan diffusivity $Đ_1$ with occupancy is that it is independent of molecular loading within the zeolite.

$$Đ_1 = Đ_1(0) \tag{26}$$

This is indeed found to be true in several cases [22,40,41]. As illustration of this behaviour see Fig. 17a for diffusion of n-heptane in 5A. However, in other cases $Đ_1$ decreases with increasing loading within the zeolite; see data in Fig. 17b for diffusion of n-heptane in 13X. It appears that increased occupancy leads to a hindering effect. The experimental data of Ruthven and Doetsch [40] for n-heptane in 13X appears to follow a simple relationship

$$Đ = Đ_1(0)\left(1-\frac{\Theta_1}{\Theta_{\text{sat}}}\right)^8 = Đ_1(0)(1-\theta_1)^8 \tag{27}$$

where we have taken Θ_{sat} = four molecules per unit cage. Fig. 17c compares Eq. (27) with the experimental data; we see that the agreement is very good. The value of the exponent 8 can perhaps be interpreted as the number of nearest neighbour sites. The exponent in Eq. (27) will therefore depend on the particular molecule and the specified zeolite structure. Paschek and Krishna [42] have performed Monte Carlo simulations for diffusion of 2-methyl hexane in silicalite and found that $Đ_1 = Đ_1(0)(1-\theta_1)$.

Diffusion within a zeolite structure is an activated process and this is evidenced by the fact that the Maxwell–Stefan diffusivity follows an Arrhenius temperature dependence. Fig. 17d shows some experimental data to demonstrate the validity of the Arrhenius dependence.

3.4. Diffusion of multicomponent mixtures within a zeolite

In order to extend the analysis to two or more components diffusing within a zeolite, we draw inspiration from the Maxwell–Stefan equations developed for bulk fluid mixtures [21,24,28]. In writing the appropriate equations for diffusion of n components within a zeolite we treat the zeolite

itself as species $(n+1)$ and consider the fractional occupancies to be the analogue of the mole fractions. Following the treatment of Kapteijn et al. [24] we write

$$-\rho\frac{\theta_i}{RT}\nabla\mu_i=\sum_{\substack{j=1\\ j\neq i}}^{n}\frac{\Theta_j\mathbf{N}_i-\Theta_i\mathbf{N}_j}{\Theta_{i,\mathrm{sat}}\Theta_{j,\mathrm{sat}}Đ_{ij}}+\frac{\mathbf{N}_i}{\Theta_{i,\mathrm{sat}}Đ_i};\quad i=1,\ 2,\ \ldots,\ n \tag{28}$$

In the Maxwell–Stefan formulation for zeolite diffusion (Eq. (28)) we have to reckon in general with two types of Maxwell–Stefan diffusivities, $Đ_{ij}$ and $Đ_i$. The $Đ_i$ are the same diffusivites as encountered earlier when we considered single component diffusion. Mixture diffusion introduces an additional complication due to sorbate–sorbate interactions. This interaction is embodied in the coefficients $Đ_{ij}$. We can consider this coefficient as representing the facility for counter-exchange, i.e. at a sorption site the sorbed species j is replaced by the species i. The net effect of this counter-exchange is a slowing down of a faster moving species due to interactions with a species of lower mobility. Also, a species of lower mobility is accelerated by interactions with another species of higher mobility. In the foregoing discussions we view the mobility as reflected in the coefficient $Đ_i$. The two types of Maxwell–Stefan diffusivities are portrayed in Fig. 18. In the inset to Fig. 18 we portray $Đ_{12}$ as representing the ease with which species 1 is replaced by species 2.

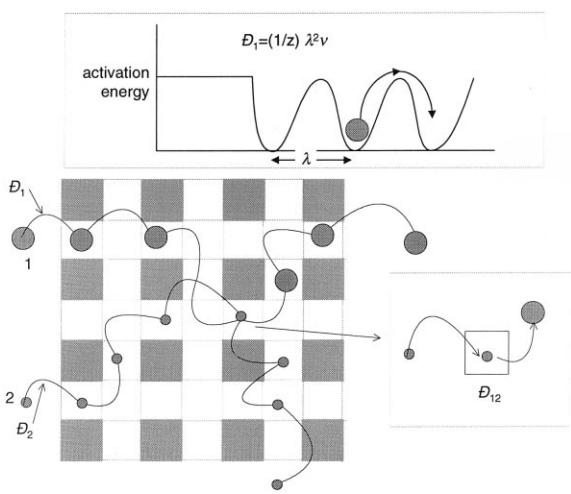

Fig. 18. Pictorial representation of the Maxwell–Stefan diffusivities.

There are no fundamental models as yet to predict the counter-exchange coefficient $Đ_{ij}$. A procedure for the estimation of the counter-sorption diffusivity has been suggested by Krishna [25] based on the generalisation of Vignes [43] relationship for diffusion in bulk liquid mixtures

$$Đ_{ij}=[Đ_i]^{\theta_i/(\theta_i+\theta_j)}[Đ_j]^{\theta_j/(\theta_i+\theta_j)} \tag{29}$$

which is essentially a logarithmic interpolation formula between the values of $Đ_i$ and $Đ_j$. We will seek validation of Eq. (29) a little later in this paper. It cannot be overstressed that the important advantage of the Maxwell–Stefan formulation is that the mixture diffusion behaviour can be estimated on the basis of information on the mobilities of the pure components, $Đ_i$ $(i=1, 2, \ldots, n)$.

The chemical potential gradients in Eq. (28) may be expressed in terms of the gradients of the occupancies by introduction of the matrix of thermodynamic factors $[\Gamma]$

$$\frac{\theta_i}{RT}\nabla\mu_i=\sum_{j=1}^{n}\Gamma_{ij}\nabla\theta_j;\quad \Gamma_{ij}\equiv\left(\frac{\Theta_{j,\mathrm{sat}}}{\Theta_{i,\mathrm{sat}}}\right)\frac{\Theta_i}{p_i}\frac{\partial p_i}{\partial\Theta_j};\quad i,\ j=1,\ 2,\ \ldots,\ n \tag{30}$$

The elements of $[\Gamma]$ have to be determined by (numerical) differentiation of the IAST or RAST isotherm models described by Eqs. (4)–(9).

Combining Eqs. (28) and (30) we can write down an explicit expression for the fluxes $\mathbf{N}_i$ using n-dimensional matrix notation

$$(\mathbf{N})=-\rho[\Theta_{\mathrm{sat}}][B]^{-1}[\Gamma]\nabla(\theta) \tag{31}$$

where the elements of the matrix $[B]$ are

$$B_{ii}=\frac{1}{Đ_i}+\sum_{\substack{j=1\\ j\neq i}}^{n}\frac{\theta_j}{Đ_{ij}};\quad B_{ij}=-\frac{\theta_i}{Đ_{ij}};\quad i,\ j=1,\ 2,\ \ldots,\ n \tag{32}$$

and $[\Theta_{\mathrm{sat}}]$ is a diagonal matrix of saturation capacities:

$$[\Theta_{\text{sat}}] = \begin{bmatrix} \Theta_{1,\text{sat}} & 0 & 0 & 0 \\ 0 & \Theta_{2,\text{sat}} & 0 & 0 \\ 0 & 0 & \ddots & 0 \\ 0 & 0 & 0 & \Theta_{n,\text{sat}} \end{bmatrix} \tag{33}$$

The more commonly used Fick diffusivity matrix is defined as

$$(\mathbf{N}) = -\rho[\Theta_{\text{sat}}][D]\nabla(\theta) \tag{34}$$

Comparing Eqs. (31) and (34) we obtain the following inter-relation between the Fick and the Maxwell–Stefan diffusivities

$$[D] = [B]^{-1}[\Gamma]; \quad [B]^{-1} = [D][\Gamma]^{-1} \tag{35}$$

which is the n-component analogue of Eq. (21). For the case where the interchange coefficient $Đ_{ij}$ is fast enough not to be a limiting factor, i.e.

$$\frac{1}{Đ_{ij}} \to 0; \quad Đ_{ij} \to \infty; \quad i, j = 1, 2, \ldots, n \tag{36}$$

Eqs. (31)–(35) simplify to yield

$$[D] = \begin{bmatrix} Đ_1 & 0 & 0 & 0 \\ 0 & Đ_2 & 0 & 0 \\ 0 & 0 & \ddots & 0 \\ 0 & 0 & 0 & Đ_n \end{bmatrix} [\Gamma];$$

$$(\mathbf{N}) = -\rho \begin{bmatrix} \Theta_{1,\text{sat}} & 0 & 0 & 0 \\ 0 & \Theta_{2,\text{sat}} & 0 & 0 \\ 0 & 0 & \ddots & 0 \\ 0 & 0 & 0 & \Theta_{n,\text{sat}} \end{bmatrix} \begin{bmatrix} Đ_1 & 0 & 0 & 0 \\ 0 & Đ_2 & 0 & 0 \\ 0 & 0 & \ddots & 0 \\ 0 & 0 & 0 & Đ_n \end{bmatrix}$$

$$[\Gamma]\nabla(\theta) \tag{37}$$

The thermodynamic correction factor matrix $[\Gamma]$ is generally non-diagonal and has a significant influence on the diffusion behaviour of mixtures.

For a binary mixture, we could force-fit Eq. (34) for the two fluxes $\mathbf{N}_i$ into the form of Fick's law for each species:

$$\mathbf{N}_i = -\rho\Theta_{i,\text{sat}}D_{i,\text{eff}}\nabla\theta_i; \quad i = 1, 2 \tag{38}$$

where the effective Fick diffusivities of component 1 and 2 are given by

$$D_{1,\text{eff}} = D_{11} + D_{12}\frac{\nabla\theta_2}{\nabla\theta_1} \tag{39}$$

$$D_{2,\text{eff}} = D_{21}\frac{\nabla\theta_1}{\nabla\theta_2} + D_{22} \tag{40}$$

For the case where the interchange coefficient $Đ_{12}$ is fast enough not to be a limiting factor (Eq. (36)), the expressions (Eqs. (38)–(40)) for the effective Fick diffusivities simplify to give

$$D_{1,\text{eff}} = \frac{Đ_1}{(1-\theta_1-\theta_2)}\left((1-\theta_2) + \theta_1\frac{\nabla\theta_2}{\nabla\theta_1}\right) \tag{41}$$

$$D_{2,\text{eff}} = \frac{Đ_2}{(1-\theta_1-\theta_2)}\left((1-\theta_1) + \theta_2\frac{\nabla\theta_1}{\nabla\theta_2}\right) \tag{42}$$

which coincide with those given by Habgood [44,45]. While Habgood derived the above expressions specifically for a two-component system, our approach can be easily extended to the general multicomponent case starting with Eq. (34). From Eqs. (41) and (42) we see that the effective Fick diffusivities are strong functions of both concentrations and concentration gradients. Furthermore, the effective diffusivity of component 1 is affected by the concentration gradient of component 2. This makes mixture diffusion in zeolites a highly coupled and non-linear process.

In the following, we shall illustrate several interesting features of mixture diffusion across zeolite membranes by considering several examples and comparing the results with published experimental data.

3.5. Separation of light hydrocarbons using a silicalite membrane

For a 50–50 mixture of methane (1)–ethane (2) at 303 K, the IAST mixture isotherm (see Fig. 4) can be differentiated to yield the elements Γ_{ij}; see Fig. 19a. Following Van de Graaf et al. [4], who have reported data on pure component Maxwell–Stefan diffusivities within a silicalite membrane, we take $Đ_1 = 1.04 \times 10^{-9}$ and $Đ_2 = 1.5 \times 10^{-10}$ $\text{m}^2\,\text{s}^{-1}$. Assuming that these Maxwell–Stefan diffusivities are independent of loading, the matrix of the Fick diffusivities can be calculated using Eq. (35). These calculations are shown in Fig. 19b. Comparison of Fig. 19a and b shows the strong influence of Γ_{ij} on the elements D_{ij}. The

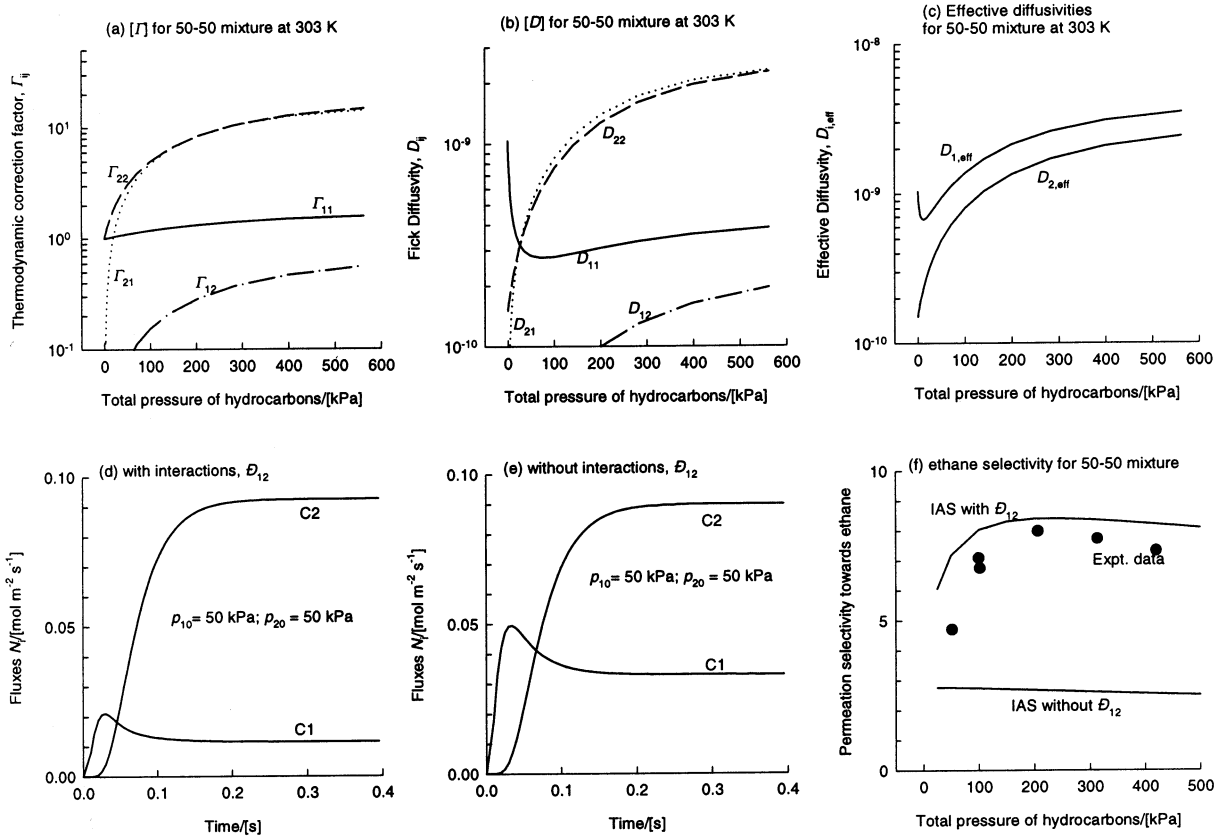

Fig. 19. (a) Thermodynamic factor matrix for the mixture of methane (1) and ethane (2) in silicalite-1 at 303 K calculated from IAS mixture isotherm. (b) Elements of the Fick diffusivity matrix taking $Đ_1 = 1.04 \times 10^{-9}$ m^2 s^{-1}, $Đ_2 = 1.5 \times 10^{-10}$ m^2 s^{-1}. (c) Effective Fick diffusivities calculated from Eqs. (39) and (40). (d) Transient fluxes for permeation across a silicalite membrane (see Fig. 20), taking $Đ_{12}$ into account. (e) Transient fluxes for permeation across a silicalite membrane (see Fig. 20), ignoring the interchange coefficient $Đ_{12}$. (f) Permeation selectivity towards ethane. Predictions of IAS–MS model with experimental data of Van de Graaf et al. [4].

effective diffusivities calculated using Eqs. (39) and (40) are shown in Fig. 19c. Note the much smaller difference between $D_{1,\mathrm{eff}}$ and $D_{2,\mathrm{eff}}$ when compared with the corresponding values of the pure component Maxwell–Stefan diffusivities $Đ_1$ and $Đ_2$.

Consider now diffusion of methane (1)–ethane (2) mixture across a silicalite membrane (Fig. 20). The upstream compartment is maintained at constant total pressure. The downstream compartment is flushed with sweep gas and we assume in the calculations below that the partial pressures of the permeating components are negligibly small, i.e. $p_{1\delta} \approx p_{2\delta} \approx 0$. The surface occupancy in the silicalite membrane (of thickness δ) is described by

$$\frac{\partial \theta_i}{\partial t} = -\frac{1}{\rho \Theta_{i,\mathrm{sat}}} \frac{\partial \mathrm{N}_i}{\partial z}; \quad \mathrm{N}_i = -\rho \Theta_{i,\mathrm{sat}} D_{i,\mathrm{eff}} \nabla \theta_i; \quad i = 1,\ 2 \tag{43}$$

The set of (coupled) partial differential equations (Eq. (43)) can be solved using the method of lines as described by Krishna and Van den Broeke [27] and Van de Graaf et al. [4]. The transient fluxes for $p_{10} = 50$ kPa, $p_{20} = 50$ kPa are shown in Fig. 19d. Neglecting the sorbate–sorbate interactions and invoking the simplification given by Eq. (36) we obtain the results shown in Fig. 19e. The steady-state selectivity

$$\text{Permeation selectivity} = \frac{\mathbf{N}_2/\mathbf{N}_1}{p_{20}/p_{10}} \quad (44)$$

is shown in Fig. 19f for the two scenarios, with and without the interactions described by $Đ_{ij}$. We note that experimental data [4] agrees very well with that predicted using IAS mixture theory along with the complete [D] matrix given by Eq. (35). This agreement is remarkable when we consider that the only experimental data inputs consist of the Maxwell–Stefan diffusivities $Đ_1$, $Đ_2$ along with the membrane parameters — silicalite matrix density, $\rho = 1.8 \times 10^6$ kg m^{-3}, membrane thickness, $\delta = 10 \times 10^{-6}$ m. The ethane selectivity predicted with the IAS theory combined with the simplified Eq. (37), neglecting $Đ_{ij}$, is much lower than that measured experimentally. The results therefore underline the need to take the complete Maxwell–Stefan formulation (Eq. (28)) into consideration.

There is another aspect of methane (1)–ethane (2) permeation which needs to be underlined. The saturation loadings of the two components, $\Theta_{i,\text{sat}}$ determined from CBMC simulations are 19 and 15 molecules per unit cell, respectively; see Table 1. The size entropy effect favours methane and therefore the ethane selectivity decreases with increasing total hydrocarbon pressure, corresponding to increasing molecular loading. Both experimental data and the IAS theory predictions show that the ethane selectivity decreases with increasing loading. The difference between the simulations presented in this paper and that of Van de Graaf [4] relates to our use of the IAST for calculating the mixture isotherms; this procedure properly takes account of the differences in the saturation capacities $\Theta_{i,\text{sat}}$ of methane and ethane. Van de Graaf [4] assumed that both the components have equal saturation capacities and employed a multicomponent Langmuir mixture isotherm. The importance of the differences in saturation capacities on permeation fluxes was first underlined by Kapteijn et al. [24].

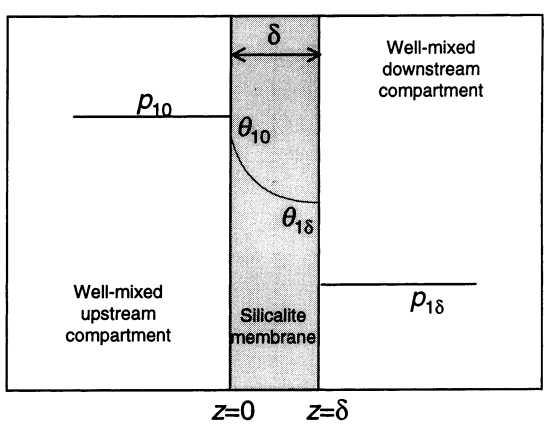

Fig. 20. Schematic view of silicalite membrane separation process for separation of hydrocarbon mixture.

Fig. 21 shows the corresponding results for permeation of the mixture methane (1)–propane (2) across a silicalite membrane at 303 K. The saturation loadings of the two components, $\Theta_{i,\text{sat}}$ determined from CBMC simulations are 19 and 12 molecules per unit cell, respectively. Size entropy effects are expected to be much more significant than that for methane–ethane mixture considered above. This is indeed seen to be the case as evidenced in the results of Fig. 21f. Both, the experimental data of Van de Graaf et al. [4] and IAS theory simulations, show that the propane selectivity decreases significantly with increasing propane partial pressure. Furthermore, the importance of the sorbate–sorbate interactions, encapsulated in $Đ_{12}$, is also strongly underlined. Comparing Fig. 21d and e we note that when taking $Đ_{12}$ into account the steady-state flux of propane is higher than that of methane. On the other hand, if we ignore $Đ_{12}$, the flux of methane is higher than that of propane. The experimental data of Van de Graaf et al. [4] support the model taking $Đ_{12}$ into account.

The curious maximum observed for the transient flux of methane for both mixtures considered in Figs. 19 and 21 is a typical phenomenon observed during transient permeation of a mixture comprising of (1) a faster moving species with low sorption strength and (2) a slower moving species but with higher sorption strength. In this mixture, the faster moving species 1 will usually exhibit a maximum flux during transient permeation. To illustrate this, we present calculations for permeation of hydrogen (1) and n-butane (2) across a silicalite membrane at 295 K. For pure component permeation, with the upstream compartment maintained at 50 kPa, the transient fluxes are

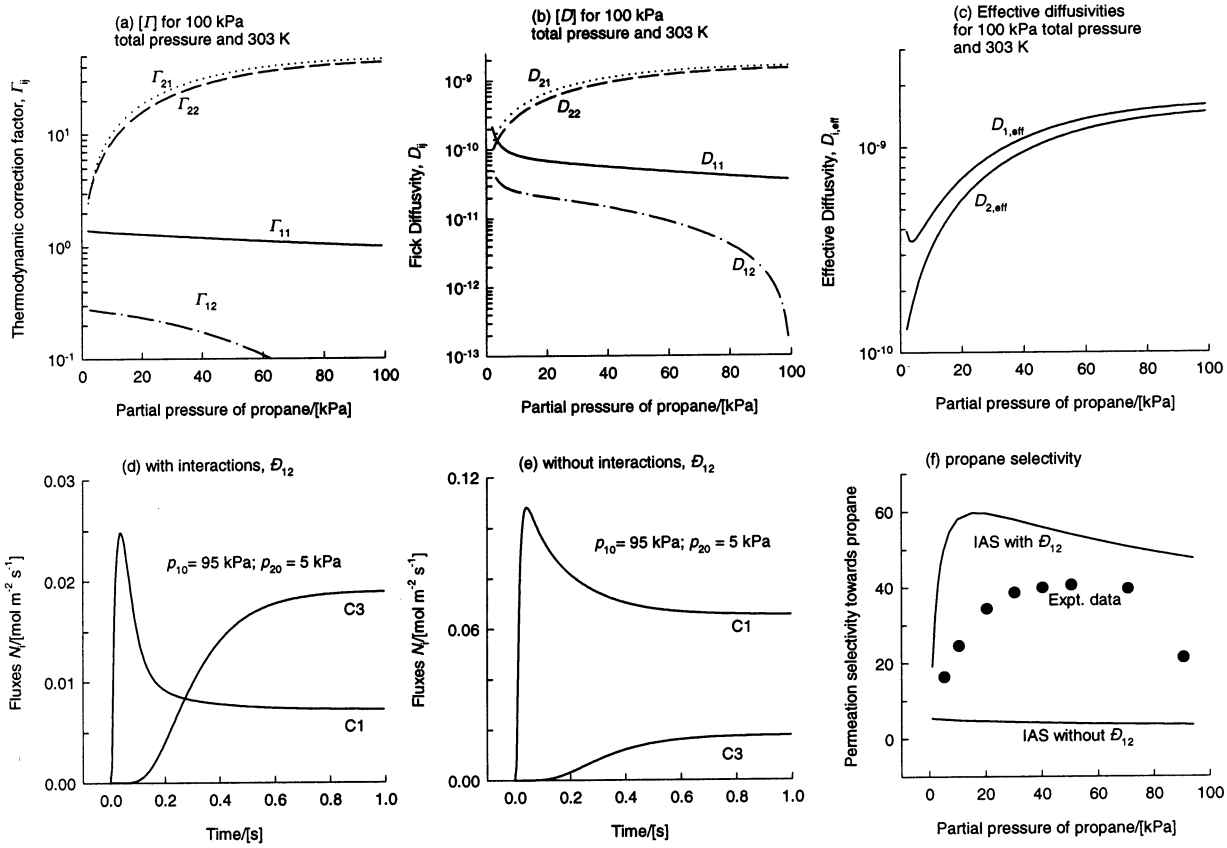

Fig. 21. (a) Thermodynamic factor matrix for the mixture of methane (1) and propane (2) in silicalite-1 at 303 K calculated from IAS mixture isotherm. (b) Elements of the Fick diffusivity matrix taking $Đ_1 = 1.04 \times 10^{-9}$ m^2 s^{-1}, $Đ_2 = 3.4 \times 10^{-11}$ m^2 s^{-1}. (c) Effective Fick diffusivities calculated from Eqs. (39) and (40). (d) Transient fluxes for permeation across a silicalite membrane (see Fig. 20), taking $Đ_{12}$ into account. (e) Transient fluxes for permeation across a silicalite membrane (see Fig. 20), ignoring the interchange coefficient $Đ_{12}$. (f) Permeation selectivity towards ethane. Predictions of IAS–MS model with experimental data of Van de Graaf et al. [41].

shown in Fig. 22a. Hydrogen has a higher steady-state flux than n-butane. The situation changes dramatically when we consider permeation of a 50–50 mixture, with partial pressures $p_{10} = p_{20} =$ 50 kPa; see Fig. 22b. Under steady-state conditions, hydrogen has a much lower flux than n-butane because it is virtually excluded from the pores of silicalite by the more strongly sorbed n-butane. Again we note the curious, sharp, maximum in the flux of the faster-moving hydrogen during the initial transience. This maximum has been experimentally confirmed by experiments reported by Kapteijn et al. [46], and provides further support of the Maxwell–Stefan formulation. The calculations for the mixture permeation fluxes in Fig. 22c have been carried out without taking $Đ_{12}$ into account. Comparison of Fig. 22b and c shows that inclusion of interchange $Đ_{12}$ has a significant impact on the magnitude of the fluxes of hydrogen.

The results seen in Fig. 22 provides the basis of a commercial process for separating hydrogen from a mixture of light hydrocarbons (methane, ethane, propane and butane) from refinery fuel gases by allowing the mixture to permeate through a carbon molecular sieve membrane [47]; see Fig. 23. The hydrocarbons are much more strongly adsorbed than hydrogen and permeate

selectively across the membrane. Propane and butanes are nearly completely removed in the permeate stream. Final purification of hydrogen by pressure swing adsorption is required before recycling back to the refinery. The advantage of this membrane separation process is that the hydrogen rich stream is recovered from the retentate (feed) side of the membrane and can be re-used in the refinery without the need for further recompression.

3.6. Separation of hexane isomers using a silicalite membrane

Consider the problem of separation of linear alkanes from branched alkanes. Branched alkanes

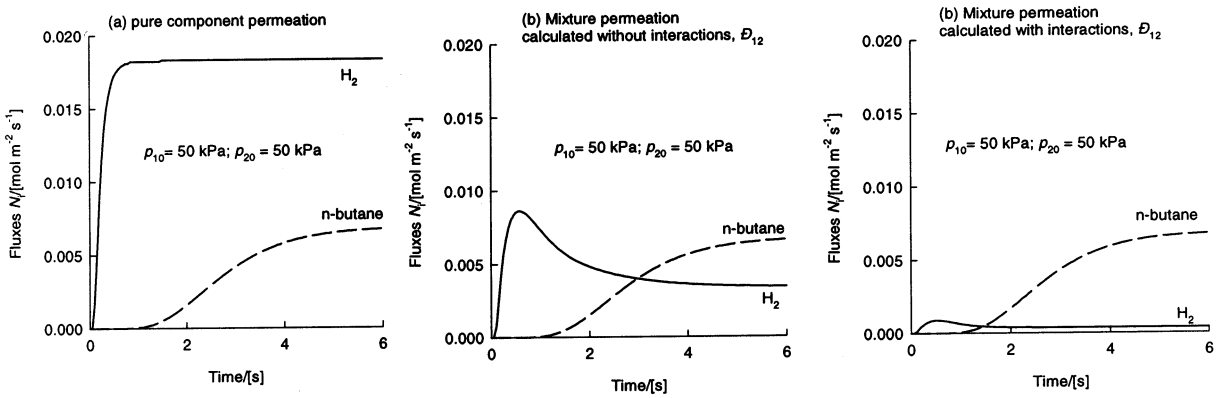

Fig. 22. (a) Transient permeation fluxes of pure components hydrogen and n-butane across a silicalite-1 membrane at 295 K. (b) Transient permeation fluxes of a 50–50 mixture of hydrogen and n-butane across a silicalite-1 membrane at 295 K. The upstream partial pressures are maintained at $p_{10} = 50$ kPa, $p_{20} = 50$ kPa. The parameters used in the calculations are silicalite matrix density, $\rho = 1800$ kg m^{-3}; membrane thickness, $\delta = 40$ μm; $q_{1,sat} = q_{2,sat} = 1.0$ mol kg^{-1} of silicalite; Langmuir parameters $b_1 = 1 \times 10^{-5}$ Pa^{-1}, $b_2 = 4 \times 10^{-4}$ Pa^{-1}; single component Maxwell–Stefan diffusivities, $Đ_1 = 1 \times 10^{-9}$ m^2 s^{-1}, $Đ_2 = 5 \times 10^{-11}$ m^2 s^{-1}. The downstream compartment is flushed with sweep gas and we assume in the calculations below that the partial pressures of the permeating components are negligibly small, i.e. $p_{1\delta} \approx p_{2\delta} \approx 0$. (c) Transient permeation fluxes calculated including the interchange coefficient $Đ_{12}$.

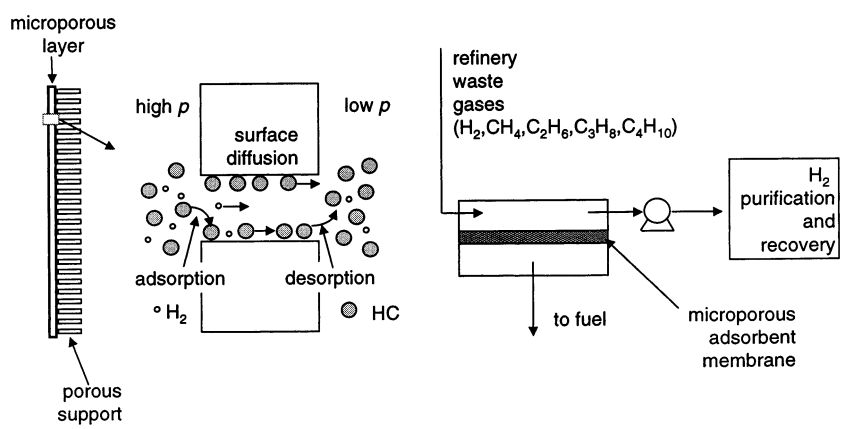

Fig. 23. A microporous carbon membrane can be used for separation of hydrocarbons from a gaseous mixture containing hydrogen. The hydrocarbons are more strongly adsorbed inside the micropores and are transported across the membrane much faster than hydrogen. Adapted from Rao and Sircar [47].

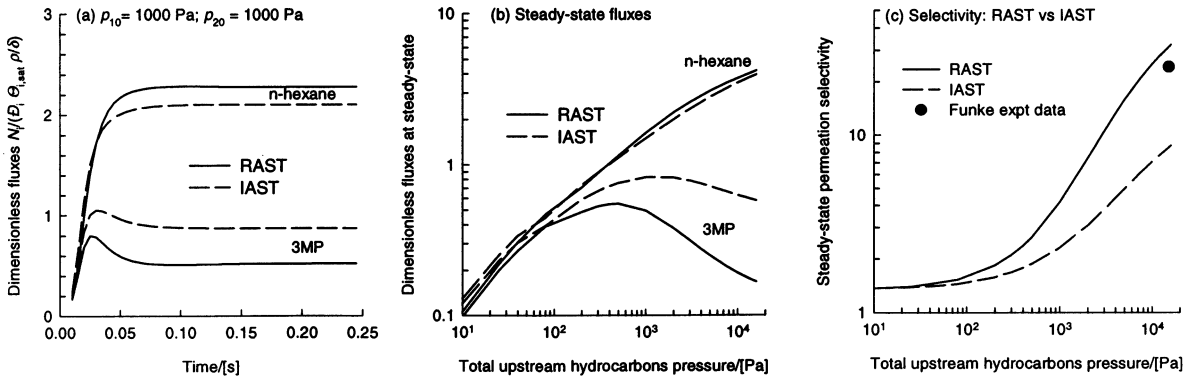

Fig. 24. (a) Transient diffusion fluxes for permeation of 50–50 mixture of n-C_6 and 3MP across a silicalite membrane at 362 K. The upstream partial pressures are $p_{10} = 5$ Pa, $p_{20} = 5$ Pa. (b) Steady-state permeation fluxes as a function of upstream hydrocarbons pressure. The Maxwell–Stefan diffusivities of the isomers are taken to be equal, i.e.$\mathcal{D}_1/\mathcal{D}_2$. (c) Separation selectivities as function of upstream hydrocarbon pressure. The experimental data point in (c) is from Funke et al. [3].

are preferred to linear alkanes as ingredients in petrol because the branched hydrocarbons burn more efficiently and have a higher octane number. Catalytic isomerisation is used to convert straight-chain hydrocarbons to their mono- or di-branched structures. However, the product of catalytic isomerisation is a mixture of linear and branched hydrocarbons that are in thermodynamic equilibrium; this gives rise to a separation problem. As seen in Fig. 2, the sorption isotherms of branched isomers in silicalite-1 exhibit inflection behaviour and this can be exploited to develop a process to separate linear alkanes from branched alkanes [9–11]. In order to illustrate these concepts let us first consider the specific example of diffusion of a mixture of n-hexane (n-C_6, component 1) and 3-methyl pentane (3MP, component 2) through a silicalite-1 membrane at a temperature of 362 K. The 50–50 mixture isotherms, determined from CBMC simulations are shown in Fig. 9b and c calculated with RAST and IAST, respectively.

Fig. 24a shows the transient permeation fluxes of a 50–50 mixture of n-C_6 and 3MP at 362 K for $p_{10} = p_{20} = 1$ kPa, calculated according to the IAST and RAST isotherms (non-ideality parameters in Table 2). In the simulations we assume that the pure component Maxwell–Stefan diffusivities are identical for the isomers, i.e. $\mathcal{D}_1 = \mathcal{D}_2$; this assumption is a conservative one from the viewpoint of separation of the isomers as we expect the branched isomer to have a lower mobility within the silicalite structure. Since the interchange coefficient $\mathcal{D}_{12}$ has a value intermediate between $\mathcal{D}_1$ and $\mathcal{D}_2$ we must also have $\mathcal{D}_1 = \mathcal{D}_2 = \mathcal{D}_{12}$. The inclusion of mixture non-ideality tends to improve the separation selectivity with respect to n-hexane. The steady-state fluxes of n-hexane and 3MP have been plotted over a whole range of total hydrocarbon pressures in the upstream compartment in Fig. 24b. We note that the steady-state flux of 3MP exhibits a maximum at about the same pressure as the maximum experienced in the mixture isotherm; compare Fig. 9b and Fig. 24b. In order to obtain high separation selectivities the upstream pressure has to be maintained at a level such that the upstream pressures are at least 10 kPa. The selectivities have been plotted in Fig. 24c for the RAST and IAST isotherm calculations. Also shown in Fig. 24c is the experimentally observed selectivity obtained by Funke et al. [3]. The RAST isotherm calculations conform more closely with the experiment; this result underlines the necessity of taking into account the mixture non-ideality effects.

We now consider diffusion of a 50–50 mixture of n-hexane and its isomer 22DMB across a silicalite membrane at a temperature of 398 K for which the isotherm has been shown in Fig. 12.Fig. 25a compares the 22DMB flux measured by Gump et al. [5] with the 22DMB loading calculated from CBMC simulations. The curious maxi-

mum in the flux of 22DMB coincides precisely with the maximum in the 22DMB loading. Calculations of the steady-state 22DMB flux by using the Maxwell–Stefan theory, along with the RAST mixture isotherm is able to reproduce the flux very well; see Fig. 25b. On the other hand, using the IAST mixture rule along with the Maxwell–Stefan theory gives a poorer representation of the 22DMB flux, stressing the need to take mixture non-idealities into account.

4. Concluding remarks

In this paper we have demonstrated the power of CBMC simulations, in conjunction with the Maxwell–Stefan diffusion theory, for modelling separations of hydrocarbon mixtures.

The following major conclusions can be drawn:

1. For mixtures of light hydrocarbons methane–ethane, methane–propane and ethane–propane, the mixture isotherms calculated from CBMC simulations are in excellent agreement with calculations using the IAS theory.
2. Size entropy effects affect the separation selectivities of methane–ethane and methane–propane mixtures.
3. For the other mixtures considered — n-butane-iso-butane, n-hexane–3MP, n-hexane–22DMB, iso-butane–propane, n-pentane–2MP, mixture non-ideality effects are important. Also, for these mixtures both size and configurational entropy effects determine separation selectivities.
4. Mixture non-ideality effects have a significant influence on separation selectivities, as demonstrated by the separation of hexane isomers.

In view of the near quantitative agreement obtained between model predictions and experimental data, we would suggest the use of our model in screening new separation concepts.

Acknowledgements

RK and DP acknowledge a grant *programma-subsidie* from the Netherlands Organisation for Scientific Research (NWO). The CBMC simulations were carried out using the BIGMAC program, authored by T.J.H. Vlugt and available on the web: http://molsim.chem.uva.nl/bigmac/. T.J.H. Vlugt is gratefully acknowledged for assistance in preparing the input data for CBMC simulations. J.M. van Baten provided valuable programming assistance.

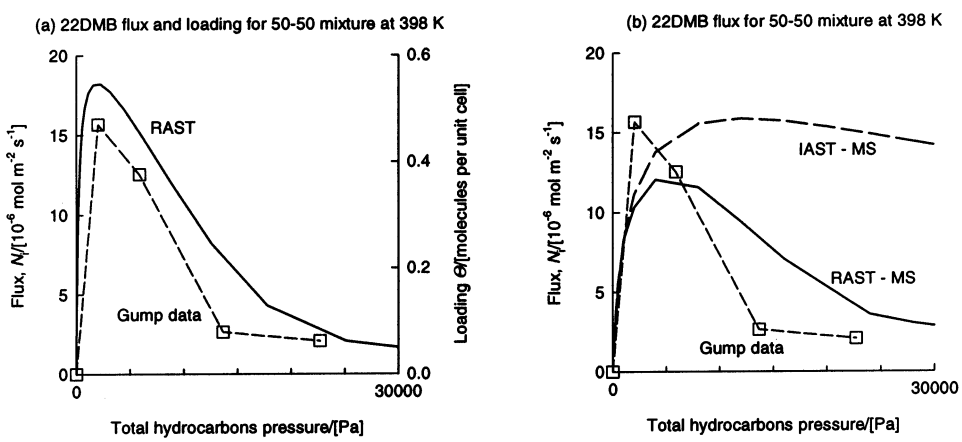

Fig. 25. Steady-state 22DMB flux for permeation of 50–50 mixture of n-C_6 and 22DMB across a silicalite membrane at 398 K. Experimental data of Gump et al. [5]. Parameter values, $\rho Đ_1/\delta = 5 \times 10^{-6}$; $Đ_1/Đ_2 = 3.5$. The continuous lines and dashed lines are predictions of the RAS and IAS theories, respectively.

References

[1] K. Huddersman, M. Klimczyk, Separation of branched hexane isomers using zeolite molecular sieves, AIChE. J. 42 (1996) 405–408.

[2] D.M. Ruthven, S. Farooq, K.S. Knaebel, Pressure Swing Adsorption, VCH Publishers, New York, 1994.

[3] H.H. Funke, A.M. Argo, J.L. Falconer, R.M. Noble, Separation of cyclic, branched, and linear hydrocarbon mixtures through silicalite membranes, Ind. Eng. Chem. Res. 36 (1997) 137–143.

[4] J. Van de Graaf, F. Kapteijn, J.A. Moulijn, Modeling permeation of binary mixtures through zeolite membranes, AIChE J. 45 (1999) 497–511.

[5] C.J. Gump, R.D. Noble, J.L. Falconer, Separation of hexane isomers through nonzeolite pores in ZSM-5 zeolite membranes, Ind. Eng. Chem. Res. 38 (1999) 2775–2781.

[6] M.S. Sun, O. Talu, D.B. Shah, Adsorption equilibria of C_5–C_{10} normal alkanes in silicalite crystals, J. Phys. Chem. 100 (1996) 17276–17280.

[7] M.S. Sun, D.B. Shah, H.H. Xu, O. Talu, Adsorption equilibria of C_1–C_4 alkanes, CO_2 and SF_6 on silicalite, J. Phys. Chem. 102 (1998) 1466–1473.

[8] Z. Du, G. Manos, T.J.H. Vlugt, B. Smit, Molecular simulation of adsorption of short linear alkanes and their mixtures in silicalite, AIChE J. 44 (1998) 1756–1764.

[9] R. Krishna, B. Smit, T.J.H. Vlugt, Sorption-induced diffusion-selective separation of hydrocarbon isomers using silicalite, J. Phys. Chem. A 102 (1998) 7727–7730.

[10] R. Krishna, B. Smit, T.J.H. Vlugt, Influence of isotherm inflection on diffusion in silicalite, Chem. Eng. Sci. 54 (1999) 1751–1757.

[11] R. Krishna, D. Paschek, Permeation of hexane isomers across ZSM-5 zeolite membranes, Ind. Eng. Chem. Res., 39 (2000) 2618–2622.

[12] B. Smit, T.L.M. Maesen, Commensurate 'freezing' of alkanes in the channels of a zeolite, Nature 374 (1995) 42–44.

[13] T.J.H. Vlugt, M.G. Martin, J.I. Siepmann, B. Smit, R. Krishna, Improving the efficiency of the CBMC algorithm, Mol. Phys. 94 (1998) 727–733.

[14] T.J.H. Vlugt, W. Zhu, F. Kapteijn, J.A. Moulijn, B. Smit, R. Krishna, Adsorption of linear and branched alkanes in the zeolite silicalite-1, J. Am. Chem. Soc. 120 (1998) 5599–5600.

[15] T.J.H. Vlugt, R. Krishna, B. Smit, Molecular simulations of adsorption isotherms of linear and branched alkanes and their mixtures in silicalite, J. Phys. Chem. B 103 (1999) 1102–1118.

[16] T.J.H. Vlugt, B. Smit, R. Krishna, Adsorption of linear and branched alkanes in ferrierite: a computational study, in: M.M.J. Treacy, B.K. Marcus, M.E. Bisher, J.B. Higgins (Eds.), Proceedings of the 12th International Zeolite Conference, vol. 1, Materials Research Society, Warrendale, PA, 1999, pp. 325–332.

[17] A.L. Myers, J.M. Prausnitz, Thermodynamics of mixed gas adsorption, AIChE J. 11 (1965) 121–130.

[18] G. Calleja, A. Jimenez, J. Pau, L. Dominguez, P. Perez, Multicomponent adsorption equilibrium of ethylene, propane, propylene and CO_2 on 13X zeolite, Gas Sep. Purif. 8 (1994) 247–256.

[19] J. Talbot, Analysis of adsorption selectivity in a one-dimensional model system, AIChE J. 43 (1997) 2471–2478.

[20] R.B. Bird, W.E. Stewart, E.N. Lightfoot, Transport Phenomena, Wiley, New York, 1960.

[21] R. Taylor, R. Krishna, Multicomponent Mass Transfer, Wiley, New York, 1993.

[22] J. Kärger, D.M. Ruthven, Difflusion in Zeolites, Wiley, New York, 1992.

[23] D.M. Ruthven, Principles of Adsorption and Adsorption Processes, Wiley, New York, 1984.

[24] F. Kapteijn, J.A. Moulijn, R. Krishna, The generalized Maxwell–Stefan model for diffusion in zeolites: sorbate molecules with different saturation loadings, Chem. Eng. Sci. 55 (2000) 2923–2930.

[25] R. Krishna, Multicomponent surface diffusion of adsorbed species. A description based on the generalized Maxwell–Stefan diffusion equations, Chem. Eng. Sci. 45 (1990) 1779–1791.

[26] R. Krishna, Problems and pitfalls in the use of the Fick formulation for intraparticle diffusion, Chem. Eng. Sci. 48 (1993) 845–861.

[27] R. Krishna, L.J.P. van den Broeke, The Maxwell–Stefan description of mass transport across zeolite membranes, Chem. Eng. J. 57 (1995) 155–162.

[28] R. Krishna, J.A. Wesselingh, The Maxwell–Stefan approach to mass transfer, Chem. Eng. Sci. 52 (1997) 861–911.

[29] L.J.P. Van den Broeke, S.A. Nijhuis, R. Krishna, Monte Carlo simulations of diffusion in zeolites and comparison with the generalized Maxwell–Stefan theory, J. Catal. 136 (1992) 463–477.

[30] L.J.P. Van den Broeke, R. Krishna, Experimental verification of the Maxwell–Stefan theory for micropore diffusion, Chem. Eng. Sci. 50 (1995) 2507–2522.

[31] R.M. Barrer, Zeolites and Clay Minerals as Sorbents and Molecular Sieves, Academic Press, London, 1978.

[32] C.J. Guo, O. Talu, D.T. Hayhurst, Phase transition and structural heterogeneity: benzene adsorption on silicalite, AIChE J. 35 (1989) 573–578.

[33] D.B. Shah, C.J. Guo, D.T. Hayhurst, Intracrystalline diffusion of benzene in silicalite: effect of structural heterogeneity, J. Chem. Soc. Faraday Trans. 91 (1995) 1143–1146.

[34] W. Rudzinski, J. Narkiewicz-Michalek, P. Szabelski, A.S.T. Chiang, Adsorption of aromatics in zeolite ZSM-5: a thermodynamic–calorimetric study based on the model of adsorption and heterogeneous adsorption sites, Langmuir 13 (1997) 1095–1103.

[35] E. Aust, K. Dahlke, G. Emig, Simulation of transport and self-diffusion in zeolites with the Monte Carlo method, J. Catal. 115 (1989) 86–97.

[36] D.A. Reed, G. Ehrlich, Surface diffusion, atomic jump rates and thermodynamics, Surface Sci. 102 (1981) 588–609.

[37] D.A. Reed, G. Ehrlich, Surface diffusivity and the time correlation of concentration fluctuations, Surface Sci. 105 (1981) 603–628.
[38] L. Riekert, Rates of sorption and diffusion of hydrocarbons in zeolites, AIChE J. 17 (1971) 446–454.
[39] V.P. Zhdanov, General equations for description of surface diffusion in the framework of the lattice gas model, Surface Sci. 194 (1985) L13–L17.
[40] D.M. Ruthven, I.H. Doetsch, Diffusion of hydrocarbons in 13X zeolite, AIChE J. 22 (1976) 882–886.
[41] D.M. Ruthven, M.F.M. Post, Diffusion in zeolite molecular sieves, in: H. van Bekkum, E.M. Flanigan, J.C. Jansen (Eds.), Introduction to Zeolite Science and Practice, second ed., Elsevier, Amsterdam, 2000.
[42] D. Paschek, R. Krishna, Monte Carlo simulations of self- and transport- diffusivities of 2-methylhexane in silicalite, Phys. Chem. Chem. Phys. 2 (2000) 2389–2394.
[43] A. Vignes, Diffusion in binary solutions, Ind. Eng. Chem. Fundam. 5 (1966) 189–199.
[44] H.W. Habgood, The kinetics of molecular sieve action. Sorption of nitrogen–methane mixtures by Linde molecular sieve 4A, Can. J. Chem. 36 (1958) 1384–1397.
[45] G.F. Round, H.W. Habgood, R. Newton, A numerical analysis of surface diffusion in a binary adsorbed film, Sep. Sci. 1 (1966) 219–244.
[46] E. Kapteijn, W.J.W. Bakker, L. van de Graaf, G. Zheng, J. Poppe, L.A. Moulijn, Permeation and separation behaviour of a silicalite-1 membrane, Catal. Today 25 (1995) 213–218.
[47] M.B. Rao, S. Sircar, Nanoporous carbon membrane for gas separation, Gas Sep. Purif. 7 (1993) 279–284.